

COLD DARK MATTER SUBSTRUCTURE AND GALACTIC DISKS I:
MORPHOLOGICAL SIGNATURES OF HIERARCHICAL SATELLITE ACCRETIONSTELIOS KAZANTZIDIS,¹ JAMES S. BULLOCK,² ANDREW R. ZENTNER,^{3,4,5}
ANDREY V. KRAVTSOV,³ AND LEONIDAS A. MOUSTAKAS⁶*The Astrophysical Journal, submitted*

ABSTRACT

We conduct a series of high-resolution, fully self-consistent dissipationless N -body simulations to investigate the cumulative effect of substructure mergers onto thin disk galaxies in the context of the Λ CDM paradigm of structure formation. Our simulation campaign is based on a hybrid approach combining cosmological simulations and controlled numerical experiments. Substructure mass functions, orbital distributions, internal structures, and accretion times are culled directly from cosmological simulations of galaxy-sized cold dark matter (CDM) halos. We demonstrate that accretions of massive subhalos onto the central regions of host halos, where the galactic disk resides, since $z \sim 1$ should be common occurrences. In contrast, extremely few satellites in present-day CDM halos are likely to have a significant impact on the disk structure. This is due to the fact that massive subhalos with small orbital pericenters that are most capable of strongly perturbing the disk become either tidally disrupted or suffer substantial mass loss prior to $z = 0$. One host halo merger history is subsequently used to seed controlled N -body experiments of repeated satellite impacts on an initially-thin Milky Way-type disk galaxy. These simulations track the effects of six dark matter substructures, with initial masses in the range $\sim (0.7 - 2) \times 10^{10} M_{\odot}$ ($\sim 20 - 60\%$ of the disk mass), crossing the disk in the past ~ 8 Gyr. We show that these accretion events produce several distinctive observational signatures in the stellar disk including: a long-lived, low-surface brightness, ring-like feature in the outskirts; a significant flare; a central bar; and faint filamentary structures that (spuriously) resemble tidal streams in configuration space. The final distribution of disk stars exhibits a complex vertical structure that is well-described by a standard “thin-thick” disk decomposition, where the “thick” disk component has emerged primarily as a result of the interaction with the most massive subhalo. We conclude that satellite-disk encounters of the kind expected in Λ CDM models can induce morphological features in galactic disks that are similar to those being discovered in the Milky Way, M31, and in other nearby and distant disk galaxies. These results highlight the significant role of CDM substructure in setting the structure of disk galaxies and driving galaxy evolution. Upcoming galactic structure surveys and astrometric satellites may be able to distinguish between competing cosmological models by testing whether the detailed structure of galactic disks is as excited as predicted by the CDM paradigm.

Subject headings: cosmology: theory — dark matter — galaxies: formation galaxies: dynamics — galaxies: structure — methods: numerical

1. INTRODUCTION

In the cold dark matter (CDM) paradigm of structure formation, galaxy-sized dark matter halos form via the continuous accretion of smaller systems (e.g., Blumenthal et al. 1984). Recently, an explosion of data has disclosed unexpected kinematic and structural complexity in the Milky Way (MW), its neighbors, and distant galaxies. There is a growing body of evidence from local star-count surveys that the MW has, in fact, experienced numerous accretion events.

¹ Kavli Institute for Particle Astrophysics and Cosmology; and Department of Physics; and Stanford Linear Accelerator Center, Stanford University, 2575 Sand Hill Rd, Menlo Park, CA 94025 USA; stelios@slac.stanford.edu.

² Center for Cosmology; and Department of Physics & Astronomy, The University of California at Irvine, Irvine, 4168 Reines Hall, CA 92697 USA; bullock@uci.edu.

³ Kavli Institute for Cosmological Physics; and Department of Astronomy & Astrophysics; and the Enrico Fermi Institute, The University of Chicago, 5640 South Ellis Avenue, Chicago, IL 60637 USA; zentner@kicp.uchicago.edu, andrey@oddjob.uchicago.edu.

⁴ National Science Foundation Fellow.

⁵ Present Address: Department of Physics and Astronomy, University of Pittsburgh, 100 Allen Hall, 3941 O’Hara Street, Pittsburgh, PA 15260 USA; zentner@pitt.edu.

⁶ Jet Propulsion Laboratory, California Institute of Technology, MS 169-327, 4800 Oak Grove Dr, Pasadena, CA 91109 USA; leonidas@jpl.nasa.gov.

Since the original discovery of the Sagittarius dwarf galaxy and its associated tidal stream (Ibata et al. 1994; Yanny et al. 2000; Ivezić et al. 2000; Ibata et al. 2001c,b; Majewski et al. 2003), at least 5 additional, spatially-coherent structures have been found in and around the MW (Newberg et al. 2002; Gilmore et al. 2002; Yanny et al. 2003; Martin et al. 2004; Juric et al. 2005; Martínez-Delgado et al. 2005; Grillmair 2006a,b; Grillmair & Dionatos 2006; Rocha-Pinto et al. 2006; Belokurov et al. 2006). These numbers are in general agreement with predictions of dwarf galaxy accretion and disruption in the prevailing Λ CDM cosmological model (Bullock et al. 2001; Bullock & Johnston 2005; Bell et al. 2007) and the character of the structures themselves are similar to those expected in simulations of satellite galaxy disruption (Johnston et al. 1995).

Among the more intriguing stellar structures discovered in the MW is the Monoceros Ring (Newberg et al. 2002). This coherent, low-metallicity feature spans $\sim 170^\circ$ degrees around the Galaxy and lies near the disk plane at a Galacto-centric distance of ~ 20 kpc (Newberg et al. 2002; Yanny et al. 2003; Ibata et al. 2003; Rocha-Pinto et al. 2003; Conn et al. 2005). It is unclear whether this structure is yet another example of tidal debris from an accreted dwarf galaxy (Yanny et al. 2003; Ibata et al. 2003; Helmi et al. 2003; Martin et al. 2004; Peñarrubia et al. 2005)

or a stellar extension of the disk itself (Ibata et al. 2003; Helmi et al. 2003; Momany et al. 2004; Moitinho et al. 2006; Momany et al. 2006).

In addition to revealing a complex assortment of structure in the outer disk and halo, photometric surveys are allowing a more detailed “tomography” of the MW disk itself (Juric et al. 2005; Newberg et al. 2006). Traditional “thin-thick” disk decompositions to these data yield thin disk exponential scale heights of ~ 250 pc and corresponding thick disk heights typically $\sim 2-4$ times larger (Siegel et al. 2002; Juric et al. 2005; Newberg et al. 2006). However, small but significant differences in published scale height determinations may reflect a more complicated disk structure than uniform scale height models allow (Newberg et al. 2006).

Ongoing studies in the Andromeda galaxy (M31) suggest that its history is at least as rich and complex as that of the MW (e.g., Ferguson et al. 2005; Kalirai et al. 2006; Ferguson 2007; Ibata et al. 2007, and references therein). At least one recent, high-metallicity accretion event is evidenced by the “giant stream” structure (Ibata et al. 2001a) and Spitzer MIPS imaging has revealed a nearly circular, ~ 10 kpc star-forming ring that may have been triggered by a past disk interaction (Gordon et al. 2006). Particularly intriguing is the extended ~ 40 kpc disk-like configuration of stars around M31 (Ibata et al. 2005). This extended “disk” component is clumpy, but possesses a relatively low velocity dispersion, ~ 30 km s $^{-1}$. It lags behind the rotation velocity of the standard M31 disk by ~ 40 km s $^{-1}$ and contains intermediate age stars similar to those of the thick disk of the MW (Brown et al. 2006; Faria et al. 2007). Recently, Peñarrubia et al. (2006) have investigated models where this structure is formed by a co-planar, near-circular accretion event. Though observations of stellar halos and thick disks in more distant galaxies are extremely challenging, deep imaging and star-count investigations have also revealed that these faint structures are likely ubiquitous (e.g., Sackett et al. 1994; Dalcanton & Bernstein 2002; Zibetti & Ferguson 2004; Dalcanton et al. 2005; Yoachim & Dalcanton 2006; Barth 2007; de Jong et al. 2007a).

The over-abundance of substructure in MW-sized dark matter halos has received a lot of attention in the literature, particularly regarding the problem of the “missing” galactic satellites (Klypin et al. 1999; Moore et al. 1999; Stoehr et al. 2002; Zentner & Bullock 2003; Kazantzidis et al. 2004b; Kravtsov et al. 2004; Mayer et al. 2007; Strigari et al. 2007a). It is important to emphasize that the satellites that will be most crucial for altering disk morphologies will be the few most massive systems of the entire population that are distinctly outside of the regime relevant to the substructure problem. Indeed, it can be shown that in the impulsive heating approximation the tidal effects of a subhalo population scale as $dE/dt \propto \int n(M_{\text{sat}}) M_{\text{sat}}^2 dM_{\text{sat}}$, where $n(M_{\text{sat}})$ and M_{sat} are the number density of satellites and satellite mass, respectively (White 2000). Since cosmological simulations predict that the mass function of CDM halos can be described by a power law, $n(M_{\text{sat}}) \propto M_{\text{sat}}^{-\alpha}$, with $\alpha \approx 1.8-1.9$ (Ghigna et al. 1998; Gao et al. 2004), the dynamical effects on stellar disks will be dominated by the most massive substructures expected to be luminous. Therefore, of concern are not the “missing” or “dark” subhalos, but rather the LMC and SMC-sized objects that fell into the disk over the past ~ 8 Gyr and that are now (presumably) dispersed throughout the Galaxy as part of its stellar halo (e.g., Bullock & Johnston 2005; Abadi et al. 2006).

In the present paper we examine the morphological signatures that substructure induces in thin galactic disks in the context of the CDM model of structure formation. Rather than focus on the stellar material liberated from accreted dwarf galaxies, we focus on the effects of satellite halo impacts on disk galaxies themselves. Specifically, we bombard an initially-thin MW-type disk galaxy with dark matter subhalos whose mass functions, orbital distributions, internal structures, and accretion times have been culled directly from cosmological simulations of MW-sized dark matter halos and study the ramifications of such encounters for disk structure.

Disk galaxies have been notoriously difficult to form in Λ CDM cosmological simulations (e.g., Navarro et al. 1995). This difficulty in conjunction with the prevalence of disks in the universe might point to an issue of fundamental cosmological importance. For example, the dark matter may not be cold or the power spectrum may not be hierarchical on small scales (e.g., Sommer-Larsen & Dolgov 2001; Zentner & Bullock 2003; Strigari et al. 2007b). However, another possibility is that current Λ CDM cosmological simulations lack the physics and/or resolution necessary to form disks. Indeed, more recent, higher resolution studies with new astrophysical inputs have been more successful (e.g., Weil et al. 1998; Thacker & Couchman 2001; Abadi et al. 2003; Sommer-Larsen et al. 2003; Governato et al. 2004; Brook et al. 2004; Robertson et al. 2004; Governato et al. 2007). Nonetheless, the problem of disk galaxy formation within a hierarchical cosmology is far from being resolved, and any successes are strongly dependent on poorly understood subgrid physics.

Additionally, despite the continuing increase in dynamic range, limited numerical resolution renders current cosmological simulations inadequate to address fully problems that encompass the enormous range of dynamical scales involved in studies of satellite-disk interactions. Given this fact and the uncertainties regarding *ab initio* formation of disk galaxies, we are motivated to explore the interplay between CDM substructure and galactic disks using *controlled N*-body simulations. Such investigations can have profound implications for our current understanding of galaxy formation and evolution.

Our work is informed considerably by many past numerical investigations into the resilience of galactic disks to infalling satellites (Quinn & Goodman 1986; Quinn et al. 1993; Walker et al. 1996; Huang & Carlberg 1997; Sellwood et al. 1998; Velazquez & White 1999; Font et al. 2001; Ardi et al. 2003; Gauthier et al. 2006; Hayashi & Chiba 2006) and we present a more direct comparison to these studies in a companion paper (Kazantzidis et al. 2007, Paper II). Successes notwithstanding, a significant fraction of these earlier numerical investigations had the drawback of not being fully self-consistent, modeling various components of the primary disk galaxy and sometimes also the satellites as rigid potentials, and focusing on experiments with infalling systems on nearly circular orbits which are poor approximations of the highly eccentric orbits that typify the trajectories of CDM substructure.

Moreover, most of the numerical work published to date considered the encounters of *single* satellites with larger multi-component disk galaxies. Notable exceptions are the studies of Font et al. (2001) and Gauthier et al. (2006), who utilized the *present-day* properties of a large ensemble of dark matter subhalos in order to investigate the dynamical effects of substructure on stellar disks. However, satellite populations possess vastly different properties at earlier times

(e.g., Zentner & Bullock 2003; Gao et al. 2004; Zentner et al. 2005a) and investigations based on the $z = 0$ substructure do not account for previous encounters of since disrupted systems with the disk. Elucidating the effects of CDM substructure on galactic disks clearly requires a more realistic treatment of the evolution of the subhalo populations.

Our numerical experiments extend and expand upon those of earlier studies in at least three major respects. We adopt for the first time a model in which the subhalo populations are truly representative of those accreted and possibly destroyed in the past, instead of the $z = 0$ *surviving* substructure present in a CDM halo. In particular, our method tracks the host halo accretion events since $z = 1$, and as discussed below, this results in a considerably larger number of important satellite-disk interactions than previously considered. Second, we employ self-consistent satellite models whose masses, internal structures, and orbital parameters are directly extracted from high-resolution cosmological N -body simulations of galaxy-sized CDM halos. This element of the modeling allow us to model the internal properties and impact parameters of the infalling systems without the need for arbitrary choices.

Finally, the primary disk galaxy models are motivated by the prevailing Λ CDM paradigm of structure formation and are derived from explicit distribution functions. In addition, they are flexible enough to permit detailed modeling of actual galaxies including the MW and M31. In the present study we adopt a model that satisfies a broad range of observational constraints available for the MW galaxy. The self-consistency of the galaxy models in synergy with the adopted high-resolution allows us to construct equilibrium N -body models of disk galaxies that are as thin as the *old*, thin stellar disk of the MW with an *exponential* scale height of $h_z \sim 0.25 \pm 0.05$ kpc (e.g., Kent et al. 1991; Dehnen & Binney 1998; Widrow & Dubinski 2005). It is worth noting that the great majority of past investigations (e.g., Velazquez & White 1999; Font et al. 2001) considered N -body models of disk galaxies that were much thicker compared to the old, thin disk of the MW. As we demonstrate in Paper II, owing to their larger vertical velocity dispersions, thicker disks are relatively less affected by encounters with satellites compared to their thin counterparts.

We model the infalling systems as pure dark matter subhalos and do not follow the evolution (or deposition) of the *stars* in the accreted systems. Our focus, in this study, is on the evolution of the stellar material in an initially-thin disk. We demonstrate that a thin disk component may survive, even strongly perturbed, significant bombardment by halo substructure and show that a number of (sub-dominant) low-surface brightness features arise in response to these encounters. The resulting morphological signatures resemble the complex faint structures that are seen in the MW, M31, and in other nearby and distant disk galaxies. Our work suggests that complex stellar components such as the Monoceros Ring in the MW and extended M31 disk may arise naturally as disk stars are tidally heated by infalling halo substructure of the kind predicted by the Λ CDM paradigm of structure formation. These findings highlight the substantial role of CDM substructure in setting the observable structure of galactic disks and driving galaxy morphological evolution.

The outline of this paper is as follows. In Section 2 we use cosmological simulations to study substructure properties and accretion statistics in four MW-sized CDM halos, select target subhalos from one halo merger history for subsequent re-simulation, and describe the controlled numerical experi-

ments to model the impact of these accretion events on the structure of a MW-type thin disk galaxy. Section 3 contains results from this simulation campaign pertaining to the global morphological evolution that infalling CDM satellites can induce in stellar disks. Implications and extensions of these findings are discussed in Section 4. Finally, in Section 5, we summarize our main results and conclusions. Note that in the remainder of the paper we use the terms “satellites,” “subhalos,” and “substructures” interchangeably.

2. NUMERICAL METHODS

The main goal of the present study is to investigate the morphological signatures created by the gravitational interaction between a population of *dark* subhalos and a thin galactic disk. We begin this section by describing cosmological numerical simulations of the formation of four MW-sized halos in the concordance Λ CDM cosmological model. In § 2.2 we analyze these simulations to quantify the frequency with which massive subhalos approach the very central regions of their hosts, where the galactic disk presumably lies. We identify one of these host halos, and in § 2.3 we extract from it the properties of individual substructures for subsequent controlled re-simulation. To be specific, we derive the orbital parameters, masses, density profiles, and accretion times of selected satellites from the cosmological simulation and use these properties to initialize controlled numerical simulations of subhalo-disk encounters. This allows us to connect the cosmological evolution of a MW-sized CDM halo with the evolution of a thin, stellar disk. In § 2.4 we introduce the primary galaxy models and the numerical methods we employ to construct them. Finally, in § 2.5 we describe in detail our simulation techniques as well as the controlled numerical experiments of the adopted halo merger history.

2.1. Hierarchical Cosmological Simulations

The cosmological halos we analyze come from two different simulations that were performed using the Adaptive Refinement Tree (ART) N -body code (Kravtsov et al. 1997; Kravtsov 1999). Both simulations assume a flat Λ CDM cosmology with $\Omega_m = 1 - \Omega_\Lambda = 0.3$, $\Omega_b = 0.043$, $h = 0.7$ and $\sigma_8 = 0.9$.

The first simulation followed the evolution of three MW-sized halos within a cubic volume of $25 h^{-1}$ Mpc on a side using the multiple mass resolution technique described in Klypin et al. (2001). We denote this simulation “L25” and the halos as “G₁”, “G₂”, and “G₃”. The mass resolution in the vicinity of each system was $m_p \simeq 1.2 \times 10^6 h^{-1} M_\odot$, corresponding to 1024^3 particles over the entire computational box, and the simulation achieved a maximum spatial resolution of $191 h^{-1}$ pc. Various properties of the L25 halos and their substructure have been discussed previously in Klypin et al. (2001), Kravtsov et al. (2004), and Zentner et al. (2005b).

The second simulation followed the evolution of a single MW-sized halo in a cubic volume of $20 h^{-1}$ Mpc on a side using the same multiple mass technique. We refer to this simulation as “L20” and the halo as “G₄”. The maximum spatial resolution for L20 was $153 h^{-1}$ pc and the mass per particle within the region of halo G₄ was $m_p \simeq 6.1 \times 10^5 h^{-1} M_\odot$, corresponding to 1024^3 particles in the entire volume. The L20 MW halo has been discussed previously in Prada et al. (2006), and Gnedin & Kravtsov (2006).

We define virial masses, M_{vir} , and radii, r_{vir} , for each host halo at $z = 0$ according to a fixed overdensity $\Delta = 337$

with respect to the mean density of the universe, $\bar{\rho}$, centered on the particle with the highest local density. This implies that virial mass and radius are related by $M_{\text{vir}} = 4\pi\Delta\bar{\rho}r_{\text{vir}}^3/3$. Halos G₁ through G₄ have virial masses $M_{\text{vir}} \simeq (1.5, 1.1, 1.1, 1.4) \times 10^{12} h^{-1}M_{\odot}$, and virial radii $r_{\text{vir}} \simeq (234, 215, 216, 230) h^{-1}\text{kpc}$. Halos G₂ and G₃ are neighbors located approximately $427 h^{-1}\text{kpc}$ from each other in a configuration that resembles that of the Local Group. Halo G₁ is relatively isolated and is ~ 2 Mpc away from the G₂-G₃ pair. All three of these halos accrete only a small fraction of their final masses and experience no major mergers at $z \lesssim 1$ (a look-back time of ≈ 8 Gyr), and therefore may reasonably host a disk galaxy. Moreover, their merger histories do not appear to be extreme compared to the expected spread in halo accretion histories measured in simulations with better statistics (e.g., Wechsler et al. 2002). We have chosen G₁ as our fiducial case for the satellite-disk interaction experiments described in § 2.5.

In order to construct mass accretion histories of the host halos and orbital trajectories of the accreted subhalos, we identified hosts and substructures at a large number of simulation outputs up to a redshift of approximately $z \approx 10$. We used 96 available simulation outputs in this interval for L25 and 148 for L20. We identified halos using a variant of the Bound Density Maxima algorithm which has been discussed extensively in the literature⁷ (Klypin et al. 1999). Virial radii are meaningless for subhalos so their radii (and masses) are defined using an outer “truncation” radius, r_{trunc} . Here we adopt r_{trunc} as the radius at which the logarithmic slope of the spherically-averaged density profile of the subhalo exceeds a critical value, $d \ln \rho(r)/d \ln r|_{r_{\text{trunc}}} = -0.5$. This criterion is based on the fact that field halo profiles are never shallower than this value, and because this definition empirically yields a good approximation to the subhalo tidal radius, r_{tid} , where the background density of the host halo equals the density of particles bound to the subhalo. We note here that the spherical approximation for substructures is fairly well justified (Moore et al. 2004; Kazantzidis et al. 2006) and that the outer profiles of subhalos typically fall off with $d \ln \rho/d \ln r < -3$ so that the bound mass converges well before the formal truncation radius is reached.

The procedure for tracking subhalo orbital trajectories was developed in Kravtsov et al. (2004) and we briefly summarize it here for completeness. The progenitor for each subhalo at a given timestep is selected using the 25% most bound particles. We search a previous output timestep for the halo with the highest common fraction of these particles and declare this system to be the primary progenitor. Many examples of such tracks for the L25 halos and a more complete description of our methods and their tests are given in Kravtsov et al. (2004) and Zentner et al. (2005b).

2.2. Encounters of CDM Substructures with Galactic Disks

We begin by demonstrating that the $z = 0$ properties of subhalo populations are strongly biased relative to the *history* of central encounters since a redshift $z = 1$. Figure 1 shows mass functions and orbital eccentricity distributions of substructure populations within the halos G₁-G₄. For this presentation, we have scaled the masses and orbital radii of all subhalos ($M \rightarrow f_m M$ and $r \rightarrow f_r r$) in order to normalize them to a single host halo mass and radius: $f_m = M_{\text{vir}}/M_h$ and

$f_r = r_{\text{vir}}/R_h$. Here, $R_h = 244.5$ kpc and $M_h = 7.35 \times 10^{11} M_{\odot}$ are the dark halo tidal radius and the dark halo mass interior to this radius of the primary MW galaxy model, which we use in the controlled satellite-disk encounter simulations described in § 2.5. The mass of the disk in this galaxy model is $M_{\text{disk}} = 3.53 \times 10^{10} M_{\odot} \approx 0.048 M_h$, and we use this number to characterize the importance of disk impacts in the figures below. Detailed description of the primary disk galaxy model will be given in § 2.4.

The left panel of Figure 1 shows cumulative mass functions of substructures with different orbital pericenters that approach the central regions of their hosts, where the galactic disk presumably lies. The mass functions are averages over all four MW-sized host halos in the cosmological simulations that we analyze. Satellite masses are measured at the epoch closest to when the subhalo first crossed inward a (scaled) infall radius of $r_{\text{inf}} = 50$ kpc from the host halo center. We define this to be the epoch that our controlled simulations initiate. The radius r_{inf} is used to select infalling satellites that are likely to have a substantial effect on the disk structure. Subhalos that remain on the outskirts of the halo will not affect the disk as significantly. We refer to satellite properties at the simulation output time nearest to the first inward crossing of r_{inf} several times in what follows.

The pericenters associated with these subhalos are estimated from the equivalent Keplerian orbits in the spherically-averaged density profile of the host. Many of these satellites are no longer present at $z = 0$ due to disruption, but were present at some earlier epoch. We also note that these mass functions are constructed taking into account that a single distinct object may pass the host halo center multiple times since $z = 1$. This panel serves to illustrate that interactions of massive subhalos with the center of the host potential where the galactic disk resides since $z = 1$ should be common occurrences in the standard Λ CDM cosmological model. Indeed, in the adopted cosmology, ~ 5 systems with masses $M_{\text{sub}} \gtrsim 0.2 M_{\text{disk}}$ cross through the central region ($r_{\text{peri}} \leq 20$ kpc) of a MW-sized halo over a ~ 8 Gyr period.

On the other hand, by examining the *present-day* substructure population of a MW-sized halo one would be led to believe that close encounters of massive subhalos with the galactic disk are very rare: on average, ~ 1 system more massive than $0.1 M_{\text{disk}}$ is expected to be on a potentially damaging orbit with $r_{\text{peri}} \leq 40$ kpc at $z = 0$. The difference between the properties of subhalo populations that were accreted in the past and those corresponding to the surviving systems is not surprising. Subhalos on highly eccentric orbits that pass closest to the host halo center are precisely those that are most likely to lose a large percentage of their mass or become tidally disrupted after pericenter crossing (e.g., Zentner & Bullock 2003; Kravtsov et al. 2004; Gao et al. 2004; Zentner et al. 2005a). As orbiting substructures continuously lose mass, the fraction of massive satellites that interact with central disks and are likely to have a significant impact on the disk structure declines with redshift so that few remain by $z = 0$.

The right panel of Figure 1 presents orbital eccentricity distributions ($R \equiv r_{\text{peri}}/r_{\text{apo}}$) for subhalos with $M_{\text{sub}} > 0.05 M_{\text{disk}}$ averaged over the same cosmological simulations. As in the left panel, results are presented for systems that have had different pericenter crossings since $z = 1$. We also show the eccentricity distribution for *all* subhalos identified at $z = 0$. This is consistent with previous studies reporting a median apocenter-to-pericenter ratio of $r_{\text{apo}}/r_{\text{peri}} = 6/1$ for present-

⁷ For completeness, we used $r_{\text{find}} = 5 h^{-1}\text{kpc}$ and $r_{\text{find}} = 2.5 h^{-1}\text{kpc}$ as the search radii in the L25 and L20 simulations, respectively.

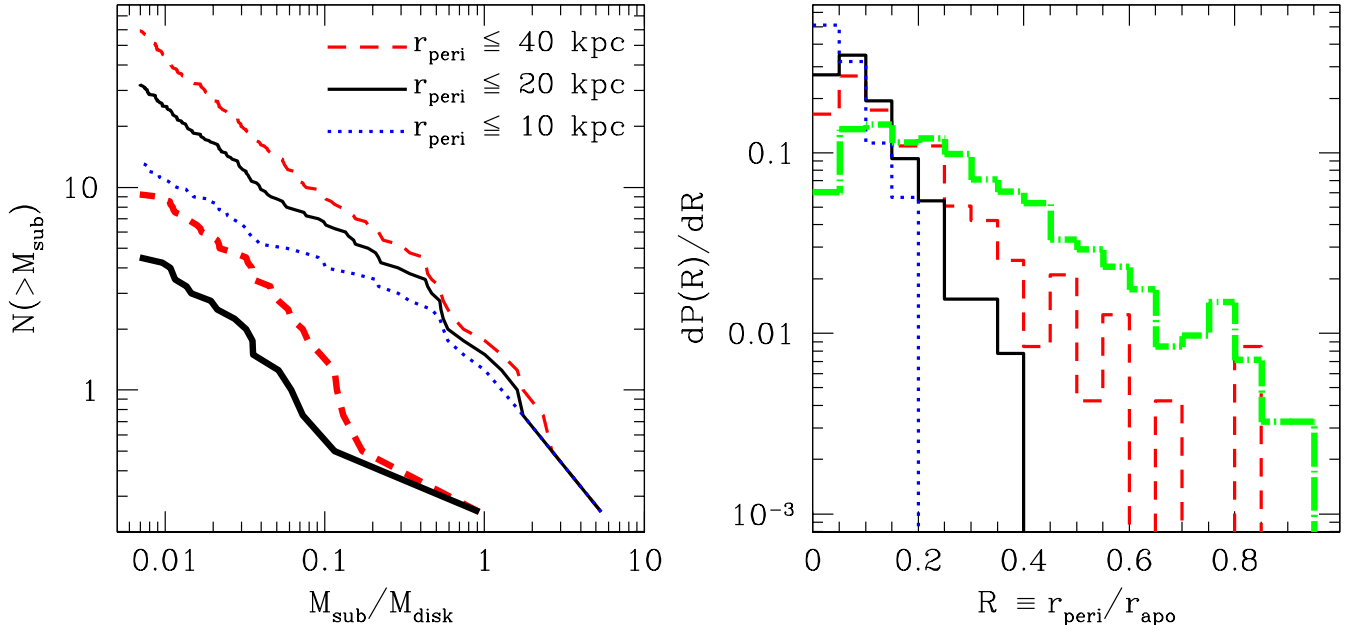


FIG. 1.— *Left*: Cumulative mass functions of subhalos that approach the central regions of their hosts averaged over four MW-sized halos formed in the Λ CDM cosmology. Upper *thin* lines present results for objects that have had pericenter crossings within 10 (*dotted*), 20 (*solid*), and 40 kpc (*dashed*) since a redshift $z = 1$. The masses are defined at the simulation output time nearest to the first inward crossing of a sphere of radius 50 kpc (in the rescaled units of the controlled simulations) and the pericenters are computed from interpolated orbits between timesteps of the simulation outputs. The lower *thick* lines correspond to the (surviving) subhalos identified at $z = 0$ with pericenters of $r_{\text{peri}} \leq 40$ kpc (*dashed*) and $r_{\text{peri}} \leq 20$ kpc (*solid*). These pericenters are also estimates based on the equivalent Keplerian orbits in the spherically-averaged density profile of the host. CDM models predict several close encounters of massive subhalos with the galactic disk since $z = 1$. In contrast, extremely few satellites in present-day subhalo populations are simultaneously massive enough and characterized by small orbital pericenters to have a profound effect on a galactic disk. *Right*: The distribution of orbital pericentric-to-apocentric distance ratios, $R \equiv r_{\text{peri}}/r_{\text{apo}}$, for subhalos with $M_{\text{sub}} > 0.05M_{\text{disk}}$. Line types for *thin* lines are as in the left panel. The *thick* dot-dashed line corresponds to the eccentricity distribution for *all* substructures at $z = 0$. Objects that have penetrated deep enough to encounter a central disk are on more radial orbits compared to those that belong to the present-day subhalo population. Note that in both panels, all units are relative to the re-scaled units of the controlled satellite-disk encounter simulations of § 2.5.

day substructure populations (e.g., Ghigna et al. 1998). The plot illuminates another bias in the properties of different subhalo populations: objects that penetrate deep into the center of the host potential are on fairly radial orbits, with $r_{\text{peri}}/r_{\text{apo}} \lesssim 0.2$, compared to the overall $z = 0$ subhalo population. It is also worth noting that circular orbits appear to be far from the norm for systems that sink into the central parts of halos and interact with galactic disks.

While not demonstrated explicitly in the panel discussed above, we find that the orbits of subhalos infalling since $z \sim 1$ are consistent with isotropic infall from a radius of 50 kpc. It is known that infall from larger radii is not isotropic (Knebe et al. 2004; Zentner et al. 2005b). However, given the limited statistical leverage of our sample and our neglect of baryonic components in shaping substructure orbits we are unable to make a more general statement regarding the directionality of satellite infall onto the disk.

2.3. Selection Criteria and Properties of Simulated Cosmological Satellites

The primary aim of this work is to investigate the morphological signatures that arise from a Λ CDM-motivated satellite accretion history. While in the previous section we have addressed the characteristics of entire subhalo populations within host halos G_1 - G_4 , here we describe the properties of the *particular* set of infalling CDM substructures that we use as the basis for the controlled subhalo-disk encounter simulations below. We choose to focus on the satellite accretion history in host halo G_1 discussed in § 2.1.

After computing the orbital tracks of all subhalos relative to the center of the primary host halo G_1 , we record all satellites that cross within a (scaled) infall radius of $r_{\text{inf}} = 50$ kpc from the host center since $z = 1$. For our re-simulation campaign, we focus on subhalos that are a significant fraction of the disk mass, but not larger than the disk itself. Figure 1 illustrates that, on average, a MW-sized dark matter halo will have ~ 1 object more massive than M_{disk} , and ~ 5 objects more massive than $0.2M_{\text{disk}}$ cross within the central 20 kpc since $z = 1$. In the present study we select satellites with $0.2M_{\text{disk}} \lesssim M_{\text{sat}} \lesssim M_{\text{disk}}$. The choice of fairly massive subhalos is motivated by the fact that they dominate the tidal heating rate by substructure. Neglecting extremely massive satellites with $M_{\text{sat}} > M_{\text{disk}}$ is conservative in this case, because we aim to study the more subtle features about a relatively well-preserved disk galaxy similar to the MW or M31. Such massive systems may well destroy or considerably alter the morphology of the disk component. In addition, very massive satellites would add substantial number of their stars to the disk thereby significantly affecting its morphology and appearance. We investigate the general robustness of thin disks to encounters with systems more massive than the ones considered here in a forthcoming study.

The final selection criterion is related to the orbital pericenters of satellites. To be specific, from the sample of selected subhalos, we choose systems which cross the central region of halo G_1 with $r_{\text{peri}} \lesssim 20$ kpc. Small pericenters are essential in order for satellites to be regarded as potentially efficient perturbers. The imposed selection criteria result in six

accreted substructures, which we denote S1-S6, to simulate over a ≈ 8 Gyr period.

One of the advantages of the present study is that the adopted subhalo models are comparatively free from assumptions associated with their internal structure. All previous numerical investigations of satellite-disk interactions employed satellite models with poorly-motivated density profiles ranging from dense γ -models to low-concentration King profiles and truncated Navarro et al. (1996, hereafter NFW) models. The contrast between low- and high-density satellites was primarily emphasized by Huang & Carlberg (1997) who argued that the latter survive tidal stripping and are accreted onto the disk, whereas the former are incorporated into outer halos. Our approach is to extract the *exact* density structures of cosmological subhalos and use them to construct high-resolution, self-consistent satellite models for the controlled simulations below.

Density profiles of selected cosmological satellites are computed at the simulation output time nearest to when the subhalo first passes within $r_{\text{inf}} = 50$ kpc of the host halo center. Subhalos S1-S6 show no sign of a central density core and are quite cuspy down to the minimum resolved radius, as expected from previous work (Kazantzidis et al. 2004b). Individual infalling substructures are modeled using a multi-parameter (α, β, γ) density profile law (Zhao 1996; Kravtsov et al. 1998). A truncation in the density profile is also introduced to mimic the effects of the host halo tidal field. This function allows a range of inner, γ , and outer, β , slopes across a fit scale radius, r_s , and includes a sharpness parameter, α , to control the nature of the transition between the two regimes. The normalization of the density profile is set by a characteristic inner density, ρ_s . From a practical perspective, truncating the profiles sharply for $r > r_{\text{tid}}$, where r_{tid} denotes the tidal radius of the satellite, results in models that are out of equilibrium. Following Kazantzidis et al. (2004b), we implement an exponential cutoff in the profile of each subhalo which sets in at the tidal radius and ensures that for $r > r_{\text{tid}}$ the density of self-bound satellite material falls off sharply. This procedure results in some additional bound mass beyond r_{tid} , the precise amount of which depends upon the adopted model parameters. In the models considered here, the mass exterior to r_{tid} is typically only about $\sim 2\%$ of the bound mass for each subhalo.

While it is cumbersome to present the detailed fits for each selected cosmological satellite here, we report that they exhibit NFW behavior in their central parts being very well approximated by a steep inner cusp of $\rho(r) \propto r^{-1}$. In contrast, the NFW profile does not provide an accurate description of the internal structure of subhalos at intermediate and large radii in agreement with previous numerical studies (Ghigna et al. 1998; Kazantzidis et al. 2004b). In all cases, the asymptotic outer slopes are found to be much steeper than -3 . This is attributable to the fact that tidal stripping from the host halo removes the outer parts of the orbiting satellites steepening their density profile. The best-fit values vary from $\beta = -3.7$ to $\beta = -4.2$ suggesting that subhalos are better represented by the Hernquist (1990) profile in their outer parts in agreement with Ghigna et al. (1998).

We follow the procedure outlined in Kazantzidis et al. (2004a) to construct self-consistent, N -body realizations of satellite models. This method is based on calculating the exact phase-space distribution function (DF) for a given density profile through an Abel transform. For the purposes of our study, we assume that the DF depends only on the binding

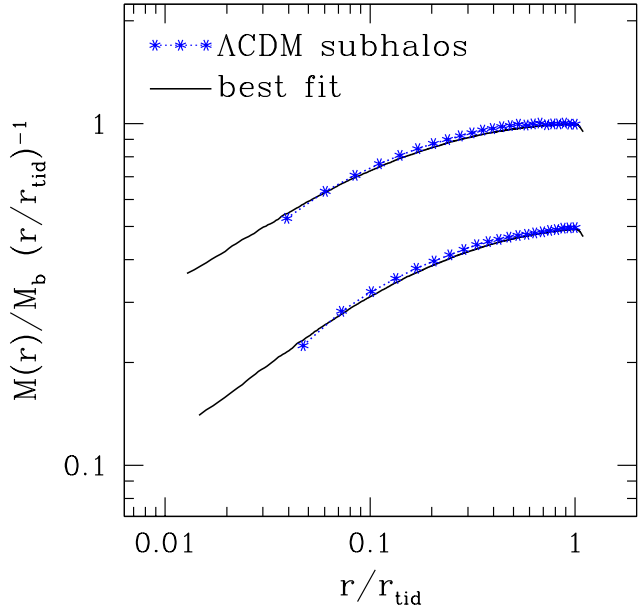


FIG. 2.— Cumulative mass profiles, $M(r)$, for representative cosmological satellites S1 and S2. Stars show profiles derived directly from the cosmological simulation of host halo G₁. Solid curves present fits to the mass distribution obtained according to the method described in the text (§2.3) and are plotted from the adopted force resolution ($2\epsilon_{\text{sat}} = 300$ pc) outward. In order to emphasize the quality of the fit, we plot the quantity $M(r)/r$ on the vertical axis rather than $M(r)$. Masses and radii are normalized to the bound mass, M_b , and tidal radius, r_{tid} , of each subhalo, respectively. For clarity, the mass profile corresponding to the lower curve is vertically shifted downward by 0.5 dex. The adopted procedure ensures that the satellite models employed in this study are initialized according to the density structure of subhalos found in high-resolution cosmological N -body simulations.

energy per unit mass, E . Numerical models of infalling substructures are then readily generated by randomly sampling the particle positions and velocities from this unique DF. A critical reader may note that satellites in the present study are modeled under the assumptions of spherical symmetry and an isotropic velocity dispersion tensor even though cosmological halos exhibit strong departures from spherical symmetry and velocity isotropy (e.g., Cole & Lacey 1996).

While this is generally correct, it has been shown that mass loss processes (tidal stripping and shocking) inside a host potential drive substructures toward shapes that are nearly spherical in both configuration and velocity space (Moore et al. 2004; Kazantzidis et al. 2006). Therefore, the assumptions of spherical symmetry and velocity isotropy for subhalos adopted here are well-grounded. Finally, the masses, positions and velocities of each selected satellite are scaled in order to correspond to the same fractions of virial quantities M_{vir} , r_{vir} , and V_{vir} , respectively, in both the parent CDM halo and in the primary galaxy model.

For each satellite model, we generate an N -body realization containing $N_{\text{sat}} = 10^6$ particles and employ a gravitational softening length of $\epsilon_{\text{sat}} = 150$ pc. This choice enables us to resolve density structures down to $\sim 1\%$ of the tidal radius of the simulated systems. The adopted particle numbers and force resolution are sufficient to resolve mass loss processes inside a host potential (Kazantzidis et al. 2004b).

In what follows, we examine whether the generous allowance for density profile shapes we considered here can give an accurate representation of the density structure of cos-

TABLE 1
PROPERTIES OF THE SATELLITE MODELS

Model	z_{acc}	t_{acc} (Gyr)	d (kpc)	$M_{\text{sat}}/M_{\text{disk}}$	r_{tid} (kpc)	V_{max} (kms $^{-1}$)	r_{max} (kpc)	r_{peri}/R_d	r_{apo}/R_d	θ ($^{\circ}$)	r_{peri}^*/R_d
(1)	(2)	(3)	(4)	(5)	(6)	(7)	(8)	(9)	(10)	(11)	(12)
S1	0.96	7.6	45.2	0.33	24.8	42.4	6.9	2.6	17.7	93.3	1.2
S2	0.89	7.3	40.7	0.57	21.5	59.8	8.1	2.6	15.7	86.6	1.2
S3	0.54	5.3	34.0	0.42	23.0	50.3	7.6	6.2	19.7	45.1	3.5
S4	0.32	3.6	28.8	0.45	19.6	41.1	4.1	0.5	10.3	59.9	1.4
S5	0.20	2.4	50.3	0.22	27.3	41.5	5.7	3.7	34.3	117.7	2.6
S6	0.11	1.4	50.5	0.21	23.2	38.8	3.7	1.1	21.6	144.5	1.9

NOTES.— Columns (2)-(10) refer to the properties of cosmological satellites recorded in the simulation output time closest to first crossing within a sphere of radius $r_{\text{inf}} = 50$ kpc from the center of host halo G_1 . Col. (1): Satellite model. Col. (2): Redshift at which satellite properties were computed. Col. (3): Look-back time in units of Gyr corresponding to the redshift of Col. (2). Col. (4): Satellite distance from the center of the host halo in kpc. Due to the finite spacing of simulation outputs this distance differs from 50 kpc. Col. (5): Bound satellite mass in units of the mass of the disk, $M_{\text{disk}} = 3.53 \times 10^{10} M_{\odot}$, used in the controlled satellite-disk encounter simulations. Col. (6): Tidal radius in kpc. Col. (7): Maximum circular velocity in kms^{-1} . Col. (8): Radius at which the maximum circular velocity occurs in kpc. Col. (9): Pericentric radius of the orbit in units of the radial scale length of the disk, $R_d = 2.82$ kpc, used in the controlled simulations. Col. (10): Apocentric radius of the orbit in units of R_d . Col. (11): Angle between the angular momentum of the satellite and the *initial* angular momentum of the disk in degrees. This angle is defined so that $\theta \sim 90^{\circ}$ represents an orbit that starts off near the pole of the disk, $\theta < 90^{\circ}$ implies a prograde orbit, and $\theta > 90^{\circ}$ corresponds to a retrograde orbit. Col. (12): Pericentric radius of the orbit in units of R_d calculated directly from the controlled simulations. This is to be compared with Col. (9).

mological subhalos. Figure 2 presents cumulative mass profiles, $M(r)$, of characteristic cosmological satellites S1 and S2 along with representations of their internal structure obtained using the density laws discussed above. Specifically, we plot the quantity $M(r)/r$, where masses and radii are normalized to the bound mass and tidal radius of each satellite, respectively. This choice scales out the gross dependence of the mass profile on radius and shows the acceptability of the fit better. Figure 2 demonstrates that the satellite models that will be used in the numerical experiments of satellite-disk interactions are initialized according to the internal structure of subhalos found in high-resolution cosmological N -body simulations.

Table 1 provides a summary of the infall times, orbital parameters, and internal structures of cosmological subhalos S1-S6 that we study in the numerical experiments of satellite-disk interactions. Columns (2)-(10) list parameters extracted directly from the cosmological simulation of host halo G_1 , and used as initial conditions in the controlled numerical experiments. We remind the reader that the structural properties for each subhalo were measured at the simulation output time closest to the first inward crossing of a sphere of radius 50 kpc (in the rescaled units of the controlled simulations). Several interesting findings regarding the properties of the simulated satellites can be read from the entries in this table.

First, the 6 different satellite models cover the mass range $0.21 < M_{\text{sat}}/M_{\text{disk}} < 0.57$, where $M_{\text{disk}} = 3.53 \times 10^{10} M_{\odot}$ is the mass of the stellar disk used in the controlled satellite-disk encounter simulations that we describe below in § 2.5. This mass range corresponds to $7.4 \times 10^9 \lesssim M_{\text{sat}}/M_{\odot} \lesssim 2 \times 10^{10}$. As we stated earlier, this mass regime is considerably larger than the regime of relevance for the missing galactic satellites problem ($\lesssim 10^9 M_{\odot}$). As a comparison, the Large Magellanic Cloud (LMC) and M32, the largest dwarf companions of MW and M31, have an estimated *total* present mass of $\sim 2 \times 10^{10} M_{\odot}$ (e.g., Schommer et al. 1992; Mastropietro et al.

2005) and $2.1 \times 10^9 M_{\odot}$ (Mateo 1998), respectively. The mass of satellites S1-S6 corresponds to the upper limit of the mass function of observed satellites in the Local Group.

Another important characteristic of the infalling subhalos is their spatial extent. Specifically, they are very extended, with $r_{\text{tid}} \gtrsim 20$ kpc, so of comparable size to the disk itself. This fact suggests that the precise pericenter or angular momentum vector of the orbit may not be particularly important in driving the disk response. We discuss this point in more detail in Paper II. Note that with the exceptions of Font et al. (2001) and Gauthier et al. (2006) all previous studies of satellite-disk interactions modeled exclusively the *compact*, baryonic cores of the infalling satellites neglecting the more diffuse dark matter component. Thus, it remains uncertain whether these earlier investigations accurately captured the amount of global morphological evolution that accreting subhalos can induce in cold stellar disks.

Table 1 also shows that the majority of infalling satellites are on fairly eccentric orbits with apocenter-to-pericenter ratio of $r_{\text{apo}}/r_{\text{peri}} > 6$. Interestingly, satellites S4 and S6 appear to be on highly radial orbits with $r_{\text{apo}}/r_{\text{peri}} \sim 20$. Moreover, as we stated earlier, our satellites are consistent with isotropic infall but the sample size is insufficient to provide significant limits on anisotropic infall. Despite this fact we note the existence of an adequate variety of recorded orbits ranging from polar (S1,S2) to prograde (S3,S4) to retrograde (S5,S6).

Finally, the orbital pericenters of the infalling systems measured directly in the satellite-disk encounter simulations are, in most cases, smaller by a factor of ~ 2 compared to those calculated from the cosmological simulation, although there are cases where the former are larger (S4 and S6). Several reasons may be responsible for these discrepancies. First, the presence of the disk in the controlled simulations provides a larger central potential compared to the dark halo alone. Secondly, the pericenters measured in the cosmological simulations are computed from the equivalent Keplerian orbits be-

cause the spacing of the simulation outputs makes several estimates of pericenters directly from orbital tracks rather poor. However, we argue that the *global* disk morphological signatures we report in this study are not sensitive to the magnitude of this difference in pericenters. The reason is that, as long as a central encounter takes place, the subhalos are so extended that their dynamical effects are felt across the entire disk nearly independently of the exact value of r_{peri} .

2.4. Primary Disk Galaxy Models

With the notable exception of Gauthier et al. (2006), all previous numerical investigations of satellite-disk interactions used approximate schemes for building N -body models of disk galaxies. In our study we employ the method of Widrow & Dubinski (2005) to construct numerical realizations of multi-component disk galaxies consisting of a thin stellar disk, a central bulge, and an extended dark matter halo. These galaxy models are derived from explicit DFs for each component and thus represent axisymmetric, equilibrium solutions to the coupled collisionless Boltzmann and Poisson equations. Because of that, this technique allows us to set up thin, equilibrium disk galaxies without instabilities and transient effects that can be present in other simpler approximate schemes (e.g., Hernquist 1993). The Widrow & Dubinski (2005) galaxy models are specified by a large number of parameters that permit detailed modeling of actual galaxies such as the MW and M31 by fitting to observational data sets.

For our experiments, we choose their best-fit model MWb, which satisfies a broad range of observational constraints available for the MW galaxy with simultaneous fits to the inner and outer rotation curve, bulge velocity dispersion, vertical force in the solar neighborhood, and total mass at large radii. The stellar disk never dominates the rotation curve of model MWb. Direct numerical simulations confirm its stability against bar formation for 10 Gyr. In what follows, we give an overview of the parameters and setup, but refer the reader to Widrow & Dubinski (2005) for a detailed discussion.

The Widrow & Dubinski (2005) disk galaxy models comprise an exponential stellar disk, a Hernquist model bulge (Hernquist 1990) and an NFW dark matter halo. The halo density distribution is given by

$$\rho_{\text{NFW}}(r) = \frac{\rho_h}{(r/r_h)(1+r/r_h)^2}, \quad (1)$$

where ρ_h is a characteristic inner density, and r_h denotes the scale radius of the profile. For convenience, the inner density ρ_h is expressed in terms of a characteristic velocity σ_h , $\rho_h \equiv \sigma_h^2/4\pi G r_h^2$, with G being the gravitational constant. The NFW density profile is formally infinite in extent with a cumulative mass that diverges as $r \rightarrow \infty$. In order to keep the total mass finite, it is necessary to truncate the profile. In practice, this is accomplished by introducing an *energy* cutoff which is described by the halo tidal radius parameter, \mathcal{E}_h ($0 < \mathcal{E}_h < 1$). This parameter controls the tidal radius of the halo, R_h , which represents the outer edge of the entire system. For model building a natural choice for the value of \mathcal{E}_h would be the one for which the resulting R_h becomes roughly equal to the cosmologically motivated virial radius, r_{vir} . Finally, arbitrary amount of rotation controlled by the parameter α_h can be added to the halo model ($\alpha_h = 1/2$ implies no rotation).

The bulge follows the Hernquist (1990) density profile

$$\rho_{\text{H}}(r) = \frac{\rho_b}{(r/a_b)(1+r/a_b)^3}, \quad (2)$$

where ρ_b and a_b are a characteristic inner density and scale length of the bulge, respectively. In analogy to the treatment of the halo, the inner density of the bulge ρ_b is expressed in terms of a characteristic velocity dispersion σ_b , $\rho_b \equiv \sigma_b^2/2\pi G a_b^2$. Similarly, the modeling of the stellar bulge is complete once the tidal radius parameter, \mathcal{E}_b , which controls the outer edge of the bulge, R_b , and the rotation parameter, α_b , are specified.

The stellar disks are assumed to be axisymmetric with density profiles $\rho_d = \rho_d(R, z)$ and DFs which are adopted directly from the self-consistent disk galaxy models of Kuijken & Dubinski (1995). The surface density profile follows an exponential distribution in cylindrical radius R , while the vertical structure is modeled by constant-thickness self-gravitating isothermal sheets (Spitzer 1942)

$$\rho_d(R, z) \propto \exp\left(-\frac{R}{R_d}\right) \text{sech}^2\left(\frac{z}{z_d}\right), \quad (3)$$

where R_d and z_d denote the radial scale length and vertical scale height of the disk, respectively. We emphasize that in the model formulation the vertical distribution of disk stars is described by a sech^2 function. Note that for $z \gtrsim z_d$, the sech^2 law mimics an exponential profile with scale height $h_z \approx z_d/2$. The construction of the stellar disk is also characterized by a truncation radius, R_{out} , and by the parameter, δR_{out} , which controls the sharpness of the truncation.

The disk phase-space DF is fully determined once the velocity ellipsoid of the disk is specified. The radial velocity dispersion, $\sigma_R(R)$, is assumed to be exponential with $\sigma_R^2(R) = \sigma_{R0}^2 \exp(-R/R_d)$, where σ_{R0} denotes the central radial velocity dispersion. The disk azimuthal dispersion, $\sigma_\phi(R)$, is related to $\sigma_R(R)$ via the epicycle approximation (Binney & Tremaine 1987), while the vertical velocity dispersion, σ_z , is set by the requirement that the adopted value of the scale height z_d is maintained in the total potential of the galaxy model. In all, the density and phase-space DFs for the three galactic components are characterized by 14 free parameters which may be tuned to fit a wide range of observational data. Given a choice of these parameters, the Widrow & Dubinski (2005) technique uses an iterative scheme to calculate the composite DF and produce equilibrium N -body models of disk galaxies.

The simulations reported here use $N_d = 10^6$ particles in the disk, $N_b = 5 \times 10^5$ in the bulge, and $N_h = 2 \times 10^6$ in the dark matter halo, and employ a gravitational softening of $\epsilon_d = 50$ pc, $\epsilon_b = 50$ pc, and $\epsilon_h = 100$ pc, respectively. Mass and force resolution are adequate to resolve the vertical structure of a thin stellar disk and minimize artificial disk heating through interactions with the massive halo particles.

Physical and numerical parameters for each of the components of the adopted primary galaxy model MWb are listed in Table 2. The best-fit value of the solar radius and the total circular velocity of the galaxy model there are given by $R_\odot \simeq 8$ kpc and $V_c(R_\odot) \approx 234$ km s $^{-1}$, respectively. The initial disk scale height is equal to $z_d = 400$ pc, consistent with the observed value for the old, thin stellar disk of the MW obtained with a variety of methods (e.g., Kent et al. 1991; Dehnen & Binney 1998; Mendez & Guzman 1998; Larsen & Humphreys 2003). Observational evidence (e.g., Quillen & Garnett 2000; Nordström et al. 2004) indicates that the scale height of the thin disk of the MW has not changed significantly over the period modeled in this study ($z \lesssim 1$). Therefore, it is reasonable to initialize the stellar disk with such thickness.

TABLE 2
PRIMARY GALAXY MODEL PARAMETERS

Component	Parameter	Value
Disk:	M_{disk}	$3.53 \times 10^{10} M_{\odot}$
	R_d	2.82 kpc
	z_d	400 pc
	R_{out}	30 kpc
	δR_{out}	1 kpc
	σ_{R0}	124.4 km s^{-1}
	$Q(2.5R_d)$	2.2
	R_{\odot}	8 kpc
	N_d	10^6
	ϵ_d	50 pc
	Bulge:	\mathcal{E}_b
σ_b		435.7 km s^{-1}
a_b		0.88 kpc
α_b		0.5
M_b		$1.18 \times 10^{10} M_{\odot}$
R_b		3.05 kpc
N_b		5×10^5
ϵ_b		50 pc
Halo:	\mathcal{E}_h	0.1
	σ_h	344.7 km s^{-1}
	r_h	8.82 kpc
	α_h	0.5
	M_h	$7.35 \times 10^{11} M_{\odot}$
	R_h	244.5 kpc
	N_h	2×10^6
	ϵ_h	100 pc

The Toomre stability parameter of the disk is equal to $Q = 2.2$ at $R = 2.5R_d$, indicating that the model is stable against local non-axisymmetric instabilities. This suggests that any significant bar growth during the satellite-disk encounter simulations can be assumed to be tidally induced by the infalling subhalos. It is also worth emphasizing that the adopted set of parameters gives $R_h = 244.5$ kpc, a value in agreement with the nominal virial radius of the MW galaxy as predicted by CDM models of cosmological structure formation (e.g., Klypin et al. 2002).

2.5. Description of Satellite-Disk Encounter Simulations

All satellite-disk encounter simulations were carried out using PKDGRAV, a multi-stepping, parallel, tree N -body code (Stadel 2001). PKDGRAV uses a spline softening length, such that the force is completely Keplerian at twice the quoted softening lengths, and multi-stepping based on the local acceleration of particles. We used an adaptive, kick-drift-kick leapfrog integrator with individual particle time steps Δt_i chosen according to $\Delta t_i \leq \eta(\epsilon_i/\alpha_i)^{1/2}$, where ϵ_i is the gravitational softening length of the particle, α_i is the value of the local acceleration, and η is a parameter that specifies the size of the individual timesteps and consequently the time accu-

racy of the integration.

For all simulations, we set the base-timestep to be equal to 1% of the orbital time of the galaxy model at the disk half-mass radius and allowed individual particle timesteps to be at most a factor of 2^{30} smaller. The number of timesteps was sufficient to accurately follow particle orbits down to the adopted force resolution of the simulations and resolve the vertical frequency of disk stars. The time integration was performed with high enough accuracy such that the total energy was conserved to better than 0.1% in all cases.

We modeled satellite impacts S1-S6 as a sequence of encounters. Starting with subhalo S1 we included subsequent systems at the epoch when they were recorded in the cosmological simulation (Table 1). Due to the fact that the simulated infalling substructures were very massive and of comparable size to the disk itself they were not introduced in the simulations directly, but rather were grown adiabatically in their orbits. This procedure ensures that the disk does not suffer substantial perturbations by the sudden presence of the satellite and change in potential at its vicinity. The mass of each satellite was increased linearly to its final value during a timescale that ranges between ~ 150 and 400 Myr depending on the subhalo mass. The disk structure was found to evolve only slightly during the growth period of each satellite.

Accreting subhalos were removed from the controlled simulations once they reached their maximum distances from the disk after crossing, and thus any given satellite was not permitted to complete a second orbit. Uniformly, these distances were only slightly smaller compared to the starting radii of the orbits. The accretion times of simulated subhalos S1-S6 (Table 1) were such that the disk interacted *simultaneously* with the first two satellites S1 and S2. We conducted an additional experiment in which subhalo S2 was introduced in the controlled simulation *after* the removal of satellite S1 and confirmed that the disk exhibited the same global evolution and morphological signatures as in the standard case.

In all of the experiments we performed, the satellites lost $\gtrsim 80\%$ of their mass after the completion of the first orbit. This justifies our decision to ignore the computationally costly, but dynamically insignificant, second (subsequent) crossing event. Note that only the *self-bound* core of each satellite was extracted from the simulations and not the unbound material, a significant fraction of which remained in the region of the disk. Removing the latter would result in potential fluctuations that could throw the disk out of equilibrium, and thus interfere with the interpretation of the results.

In order to save computational time, when time intervals between subhalo passages were larger than the timescale needed for the disk to relax after the previous interaction, we introduced the next satellite in the simulation immediately after the disk had settled from the previous encounter. Due to the complexity of the interaction, we determine this “settling” timescale empirically by monitoring basic properties of the disk structure (e.g., surface density, velocity dispersions, thickness) as a function of time. When these quantities stop evolving significantly within radii of interest ($r \lesssim 6R_d$), the encounter is deemed complete. Changes of the order of 5–10% in disk properties were considered acceptable. We note that the limiting radius of $6R_d$ is chosen because it initially contains $\sim 98\%$ of the mass of the disk. Typical settling timescales correspond to ~ 100 – 200 Myr *after* the removal of the bound core of each orbiting subhalo. This eliminates the computational expense of simulating the disk during the quiet intervals between interactions.

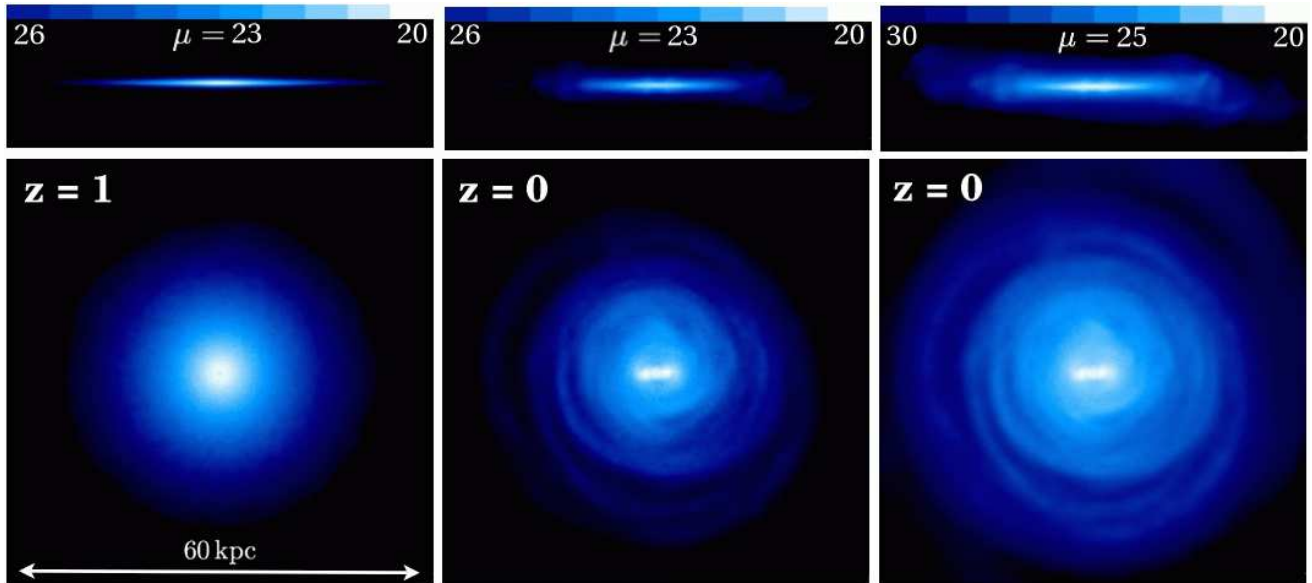


FIG. 3.— Surface brightness maps of disk stars in the simulated accretion history of host halo G_1 . The edge-on (*upper panels*) and face-on (*bottom panels*) views of the disk are displayed in each frame and the color bar in each upper panel indicates the surface brightness limits used to generate the maps. In constructing these images, a stellar mass-to-light ratio equal to $M_*/L = 3$ is assumed. Bottom images are 60 kpc on a side, while top images measure 18 kpc by 60 kpc. The *left* panel shows the initial disk assuming that the sequence of satellite-disk interactions initiates at $z = 1$. The *middle* and *right* panels depict the disk after the last satellite passage, evolved in isolation for additional ~ 4 Gyr, so that the evolution of disk stars is followed from $z = 1$ to $z = 0$. In the left and middle panels, images are shown to a limit of $\mu = 26$ mag arcsec $^{-2}$, while the right panel corresponds to a “deeper” surface brightness threshold of $\mu = 30$ mag arcsec $^{-2}$. Results are presented after centering the disk to its center of mass and rotating it to a new coordinate frame defined by the three principal axes of the total disk inertia tensor. Considerable flaring and a wealth of features that they might falsely be identified as tidal streams can be seen in the perturbed disk down to 26–30 mag arcsec $^{-2}$. The existence of non-axisymmetric structures such as extended outer rings and bars after a significant amount of time subsequent to the last accretion event confirm their robustness and indicate that axisymmetry in the disk has been destroyed and is not restored at late times.

Finally, we stress that prior to commencing the satellite-disk encounter simulations, the primary galaxy model was tilted so that the disk angular momentum vector was aligned with the angular momentum of the host CDM halo G_1 . This choice is motivated by results of cosmological simulations suggesting that the angular momenta of galaxies and their host halos tend to be well aligned (e.g., Libeskind et al. 2007).

3. RESULTS

In this section we present results regarding the evolution of an initially-thin stellar disk subject to a cosmologically-motivated subhalo merger history. Recall that we examine the disk response to substructure impacts S1-S6, which are designed to mimic a reasonable *central* accretion history for a MW-sized halo over the past ~ 8 Gyr. The “final” disk discussed in the next sections has experienced the S1-S6 encounters and was evolved in isolation for ~ 4 Gyr after the last interaction. While this allows for relaxation after the encounters, it also ensures that all of the resultant morphological features are long-lived rather than transient. Consequently, our results are relevant to systems that exhibit no obvious, ongoing encounters and have been allowed to relax in isolation.

We compute all properties of the disk and show all visualizations of the disk morphology after centering the disk to its center of mass and rotating it to a new coordinate frame defined by the three principal axes of the total disk inertia tensor. The motivation behind performing both actions is twofold. As discussed in more detail in Paper II, exchange of angular momentum between the infalling satellites and the disk tilt the disk plane substantially over the merging history and cause the disk center of mass to drift from its initial position at the origin of the coordinate frame. In the original coordinate frame, rotation in a tilted disk would appear as vertical

motion interfering with the interpretation of the results.

Finally, we underscore that there is nothing exceptional about host halo G_1 as far as the properties of the subhalo populations are concerned. In all other three MW-sized halos we analyzed, substructures of similar numbers, masses, internal structures, orbital parameters, and accretion times were identified. Though our simulation program is designed to mimic the activity in the inner halo of G_1 , the similarity of subhalo populations in all four halos suggests that the results presented next should be regarded as fairly general.

3.1. Global Disk Morphology

Figure 3 depicts the evolution of the global structure of a thin stellar disk that experiences a merging history of the type expected in Λ CDM. The left panel shows the initial configuration of disk stars assuming that the sequence of satellite-disk interactions initiates at $z = 1$, while the right and middle panels show the final configuration at $z = 0$ of the *same stars* at two different surface brightness thresholds. Stellar particles are color-coded by the projected *surface brightness*. In producing these images, we have assumed a stellar mass-to-light ratio of $M_*/L = 3$ in the V-band, as would be appropriate for an old stellar population with colors relevant for thick disks (Dalcanton & Bernstein 2002). This particular choice produces a peak edge-on central surface brightness of $\mu \sim 21$ mag arcsec $^{-2}$, similar to values seen in optical surveys of nearby, edge-on, undisturbed disk galaxies (Yoachim & Dalcanton 2006). A different choice for M_*/L would simply result in a dimming or brightening of these images and subsequent figures accordingly.

Several interesting morphological signatures of satellite-disk interactions are clear from these images. First, a wealth

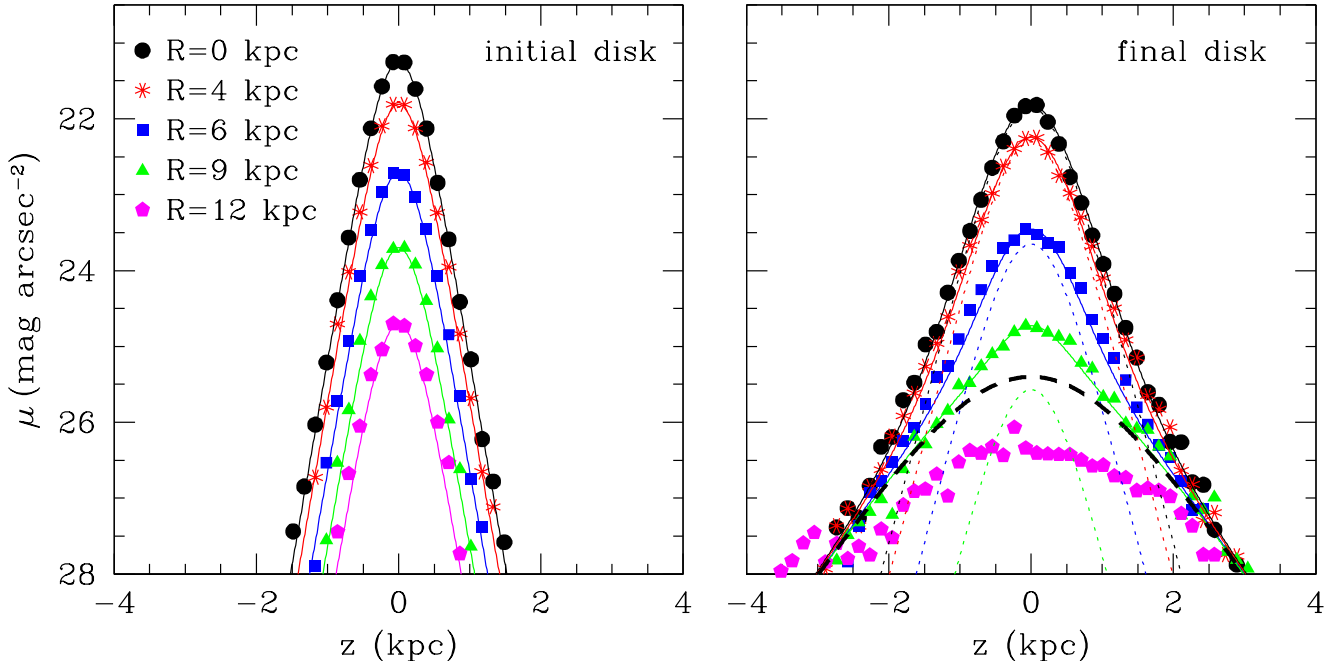


FIG. 4.— Thin-thick disk decomposition analysis. Surface brightness profiles for disk stars as a function of distance above the plane of the disk, z . The stellar distribution is observed edge-on and results are shown for both the initial (*left panel*) and final (*right panel*) disk. The final disk has experienced the S1-S6 encounters and was further evolved in isolation for ~ 4 Gyr after the last interaction to ensure that it has reached a relaxed state. Different symbols correspond to various projected radii, $|R| = 0, 4, 6, 9, 12$ kpc, averaged between the $\pm|R|$ projections about $R = 0$, and within 1 kpc strips centered on each of the projected radii. The *solid* lines in the left panel present the analytic sech^2 surface brightness profiles of the initial thin disk with $z_d = 0.4$ kpc and demonstrate a very good agreement with results obtained directly from the particle distribution. *Solid* lines in the right panel show a “thin-thick” disk decomposition for the final disk, which consists of a “thick” disk component (*dashed line*) with a sech^2 scale height of $z_{\text{thick}} = 1.6$ kpc and a “thin” disk component (*dotted lines*) with a slightly larger scale height ($z_{\text{thin}} = 0.6$ kpc) compared to that of the initial thin disk. The surface brightness profile of the “thick” disk is nearly independent of projected radius for $R < 9$ kpc explaining the existence of only one dashed line. At small projected radii ($|R| \lesssim 6$ kpc), the contribution of the thin component to the light profile of the stellar disk is dominant for heights $z \lesssim 1$ kpc. As $|R|$ increases, the situation is reversed with the thick disk component becoming prevalent. This simple decomposition provides a reasonable description of the final disk for $\mu \lesssim 27$ mag arcsec $^{-2}$ and $|R| \lesssim 9$ kpc. At fainter magnitudes and beyond $R \sim 9$ kpc, the flare and other diffuse structures become important and the adopted decomposition fails to provide an accurate description of the disk structure.

of low-surface brightness features have developed both in the plane and above the plane of the final disk as a consequence of these disturbances and we discuss these in detail in the next sections. Particularly intriguing is the presence of a conspicuous flare and non-axisymmetric structures such as extended outer rings and central bars. Their existence and robustness indicate that the axisymmetry of the disk has been destroyed by the encounters with the infalling satellites and is not restored at late times.

Moreover, as is evident in the edge-on images of the final disk in Figure 3, a high-surface brightness *thin* disk component remains after the bombardment by CDM substructure. We discuss the implication of this finding in the general context of disk survivability in a Λ CDM universe in Section 4. It is interesting to ask whether or not the bright in-plane structure would be recognized as a thin disk component in a standard disk decomposition analysis. We present such an analysis in Figure 4. This figure shows the initial and final surface brightness profiles, $\mu(z)$, of the stellar disk as a function of distance, z , above the disk plane. For this calculation, the stellar distribution is observed edge-on. Symbols correspond to different projected radii, R .

The left panel shows the analytic sech^2 surface brightness profile (eq. [3]) for the initial, thin stellar disk with a scale height of $z_d = 0.4$ kpc. By construction, there is excellent agreement between the analytic profiles and results obtained

directly from the particle distribution. As we discussed earlier, Figure 3 demonstrates that the disk is substantially perturbed by the encounters with the infalling satellites. This suggests that describing the later stages of the disk evolution requires more than the simple, single function that works well for the initial disk. Indeed, the right panel of Figure 4 presents a two-component, “thin-thick” disk decomposition for the final disk. The decomposition consists of a low-surface brightness, “thick” disk component with a sech^2 scale height of $z_{\text{thick}} = 1.6$ kpc and a sech^2 “thin” disk component with a scale height of $z_{\text{thin}} = 0.6$ kpc which is slightly larger compared to that of the initial thin disk.

This simple decomposition provides a reasonably good description of the final disk down to fairly low surface brightnesses, $\mu \lesssim 27$ mag arcsec $^{-2}$, and for $|R| \lesssim 9$ kpc. Interestingly, the edge-on thick disk component is consistent with having a surface brightness profile that is *almost* independent of projected radius for $R \lesssim 9$ kpc. At fainter magnitudes, a flare and other diffuse structures become important as discussed in § 3.2. Beyond $R \sim 9$ kpc, the adopted decomposition fails to provide an adequate representation of the disk structure. At these radii the disk is significantly flared and its structure becomes strongly irregular. The complexity of the disk structure at $R \gtrsim 9$ kpc suggests that a more complicated functional form may be needed to describe the final disk at larger radii.

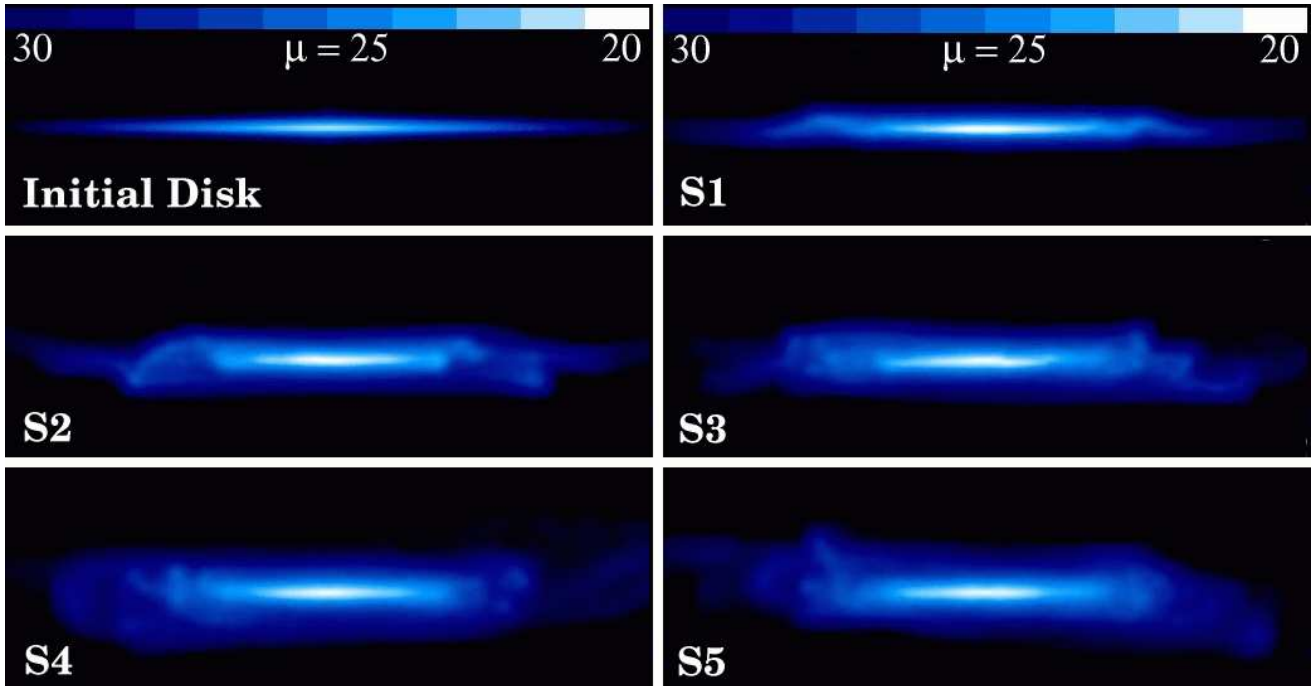


FIG. 5.— Effect of individual satellites on the global morphological evolution of the disk. Each panel shows edge-on surface brightness maps of disk stars to a surface brightness limit of $\mu \sim 30$ mag arcsec $^{-2}$ and measures 18 kpc by 60 kpc. Labels for individual satellite passages from S1 to S5 are indicated in the *lower left-hand* corners of each image and, to aid comparison, the initial disk is presented in the *upper left* panel. Images are constructed after the disk has relaxed from each encounter according to the definition in §2.5. The response to subhalo S6 can be seen in Figure 3. A high-surface brightness thin disk component is visible in all images. The first satellite passage S1 generates a warp in the outer regions of the disk. The second encounter which involves the most massive subhalo S2 causes substantial flaring above the disk plane. The remaining satellites perturb the disk structure further even though their effect is differentially less significant compared to the initial encounters. In broad terms, most of the morphological signatures have emerged as a result of the interaction with the most massive subhalo.

We note that this decomposition does not constitute a formal fit but merely provides an acceptable parametrization for the final disk structure. The analysis presented above simply serves to illustrate that the final disk cannot be represented by a *single* exponential or sech 2 function. Two components are clearly required, one of which is significantly thicker than the “thin” one. Deriving a formal fit for the disk vertical structure will not yield substantial additional information regarding the global morphological evolution of the disk, though it will be explored in the future.

Figure 4 shows a number of interesting results related to the surface brightness distributions of the final disk. First, these distributions become uniformly broader extending at considerably larger vertical distances from the disk plane compared to those of the initial thin disk. This change is caused by the encounters with the infalling subhalos and can be directly associated with the strong flare seen in the final disk which will be discussed in § 3.3. Second, the peak of the surface brightness profiles which corresponds to the light distribution in the disk plane ($z = 0$) drops systematically at all projected radii compared to that of the initial disk. This is attributable to the fact that stars are efficiently heated above the disk plane by the merging subhalos. As a result of this, the number of stars in the plane of the disk decreases with obvious consequences for the surface brightness distribution.

As the projected radius increases, the height above the plane of the disk at which the thick disk component dominates the light profile becomes progressively smaller. This is because the surface brightness distribution of the thin disk declines exponentially with R , while both the scale height, and the central (projected) surface brightness of the edge-on thick disk

vary much more slowly with radius. At small projected radii ($|R| \lesssim 6$ kpc) the thin disk component dominates for $z \lesssim 1$ kpc. However, this picture is quickly reversed. For $|R| = 9$ kpc (*triangles*) the thick disk dominates the light profile of the stellar distribution for *all* heights above the disk plane. We note that within 9 kpc, approximately $\sim 17\%$ of the final stellar mass is contained in the thick disk component.

3.2. Morphological Signatures of Satellite-Disk Encounters

The results in the previous section demonstrate that infalling CDM substructures play a significant role in setting the global morphology of a stellar disk. The face-on view of the final disk in Figure 3 (*middle and right panels*) reveals that satellite accretion can also excite strong bars which drive further evolution in the inner disk regions. The primary disk galaxy model was constructed to be stable against the formation of a bar. Thus, the observed bar growth should be regarded as tidally induced by the infalling satellites. Interestingly, the edge-on view of the same panels shows the generation of a characteristic “X” shape in the bright central disk, a finding also reported in previous numerical studies of satellite-disk encounters (Walker et al. 1996; Gauthier et al. 2006). This noticeable feature is often linked to secular evolution of galaxies driven by the presence of a bar when it buckles as a result of becoming unstable to bending modes (e.g., Combes & Sanders 1981), and may be associated with the presence of peanut-shaped bulges observed in many galaxies (e.g., Lütticke et al. 2000).

Moreover, while the bright “X”-shaped component is visible at high-surface brightness, many other interaction-driven signatures appear as low-surface brightness features. The

deep view of the final edge-on disk in Figure 3 (*right panel*) shows a number of additional filamentary structures at $\mu \gtrsim 26$ mag arcsec $^{-2}$, and other complex configurations, that develop above the disk plane. These structures bear some resemblance to tidal streams, but are in fact disk stars that have been gravitationally excited by the subhalo impacts. The final face-on disk in the same panel is also significantly more structured at faint surface brightness and large radius compared to the initial disk and is quite reminiscent of the outer disk structure seen around M31 (Ibata et al. 2005). The same image also reveals a pronounced ring-like feature at $\mu \sim 26$ mag arcsec $^{-2}$. The ring is nearly in-plane and is qualitatively similar to the Monoceros structure known to extend around the MW (Newberg et al. 2002). We emphasize that this ring is a non-transient feature which survives for a considerable amount of time after the satellite accretion events. Indeed, though this structure is generated after the interaction with satellite S2, it remains apparent at the final simulation output some ~ 4 Gyr after the final impact with subhalo S6.

Following up on the findings reported in Figs. 3 and 4, Figure 5 illustrates the effect of each satellite passage S1-S5 on the global morphological evolution of the disk. Images were created after the disk has relaxed from the encounter with each infalling subhalo according to the definition in §2.5. The high-surface brightness thin disk component discussed above is visible in all edge-on views of the disk. The first satellite passage S1 generates a pronounced warp in the disk beyond some radius. The second interaction with the most massive subhalo S2 has a dramatic effect on the disk structure causing substantial flaring above the disk plane. Subsequent satellite accretion (S3-S5) does not substantially perturb the disk further. The disk flare is visible at low surface brightness limits below 26–27 mag arcsec $^{-2}$ and becomes particularly prominent after the second impact. This fact suggests that only a fairly small number of satellites with Λ CDM motivated internal properties and orbital parameters is sufficient to generate the bulk of morphological evolution of a stellar disk. We return to this point below.

3.3. Disk Flaring

Among the most striking morphological features in the final edge-on disk is the pronounced flare, which is particularly visible at low surface brightness levels (Figures 3 and 5). A more quantitative measure of the flare induced by the accretion events in our simulations is given in Figure 6. This figure shows scale height profiles of the disk, $z(R)$, viewed edge-on. Profiles are normalized to the initial disk scale height, z_d , and are plotted as a function of projected radius in units of the disk radial scale length, R_d .

The flaring of the disk can be formally described by the increase of the vertical scale height. For the purpose of our analysis, we define the scale height at any given radius to be the vertical distance above the disk midplane where the edge-on surface brightness falls off from its maximum along the $z = 0$ disk plane by $\Delta\mu = 1$ mag arcsec $^{-2}$, $\mu(z) = \mu_0 + 1$. Though disk scale heights must be formally derived by means of fitting the particle distribution to an appropriate functional form (e.g., exponential or sech 2 law), scale heights as quantified here are well-defined and require no assumptions for their interpretation.

The left panel of Figure 6 shows scale height profiles for the initial and final disk. Results are presented using both the definition of scale height introduced above, $\mu(z) = \mu_0 + 1$, and that for which scale heights are defined to be the vertical distance

above $z = 0$ where the edge-on surface brightness falls off from the central maximum value by 2 mag arcsec $^{-2}$, $\mu(z) = \mu_0 + 2$. The final disk shows considerable flaring beyond $\sim 2 - 3R_d$ indicating that encounters with CDM substructure can be responsible for producing notable flares in stellar disks. Remarkably, the scale height of the disk near the solar radius has increased in excess of a factor of 2 as a result of the interactions with satellites S1-S6. We checked that the scale height of the same disk galaxy evolved in isolation for a timescale equal to that corresponding to the final disk (~ 8 Gyr) has grown by only about 10% indicating the quality of the initial conditions and adequate resolution of the simulations.

The right panel of Figure 6 shows the *evolution* of the scale height profile of the disk caused by individual satellite passages. After the encounter with satellite S1, the inner disk ($R \lesssim 2R_d$) appears unaffected by the accretion event despite that fact that S1 is quite massive, with an initial mass of $\sim 30\%$ of the disk mass, and is characterized by a small pericenter ($r_{\text{peri}} \sim 1.2R_d$). In contrast, the scale height of the outer disk ($R \gtrsim 3.5R_d$) raises considerably giving rise to a distinct flare. The second event, which involves the most massive satellite S2 ($M_{\text{sat}} \sim 0.6M_{\text{disk}}$), generates a stronger flare by greatly increasing the scale height of the outer disk. Though the scale height has now grown throughout the entire disk, the inner disk regions still exhibit substantial resilience to the encounter. Indeed, at $R = R_d$ the scale height only raises by $\sim 50\%$ compared to approximately a factor of 4 increase at $R = 4R_d$.

This difference in the robustness of inner and outer disks is attributed to the larger binding energy of the former and to the presence of a massive, central bulge that acts as a sink of the orbital energy of the infalling satellites. The combined effect of the remaining satellite impacts (S3-S6) on the structure of the disk is much less dramatic increasing the scale height only slightly compared to passage S2. This finding suggests that subsequent accretion events by already thickened disks induce much smaller changes in the disk scale height compared to the initial encounters. This effect was also noted previously by Quinn et al. (1993) using numerical simulations in which halos were treated as rigid potentials. In broad terms, the dynamical and morphological evolution of a galactic disk subject to a cosmologically-motivated subhalo merger history are driven by the most massive accretion event.

Given the fact that the self-gravity of the disk grows weaker as a function of distance from the center, it is not unexpected that the scale height of the final disk should increase with radius. In the thin disk approximation, we may consider the total vertical energy per unit area of the disk, $e_z = t_z + w_{dd} + w_{ds}$, where t_z is the disk vertical kinetic energy, and w_{dd} and w_{ds} are the disk potential energy densities associated with the disk self-gravity and disk-spheroid gravity, respectively (Toth & Ostriker 1992; Benson et al. 2004). In this formulation it is implicitly assumed that the spheroid includes the dark matter halo and any bulge component. For a thin disk of varying scale height, $z(R)$, we expect

$$w_{dd} = G \alpha \Sigma_d^2(R) z(R) \quad (4)$$

$$w_{ds} = G \beta \Sigma_d(R) \bar{\rho}_s(R) z^2(R). \quad (5)$$

Here, $\bar{\rho}_s(R)$ is the spheroid mass density averaged over the disk scale height at radius R and $\Sigma_d(R)$ is the projected disk surface density. The constants α and β are geometrical factors of order unity that will depend on the profile shapes of the disk and spheroid components, respectively.

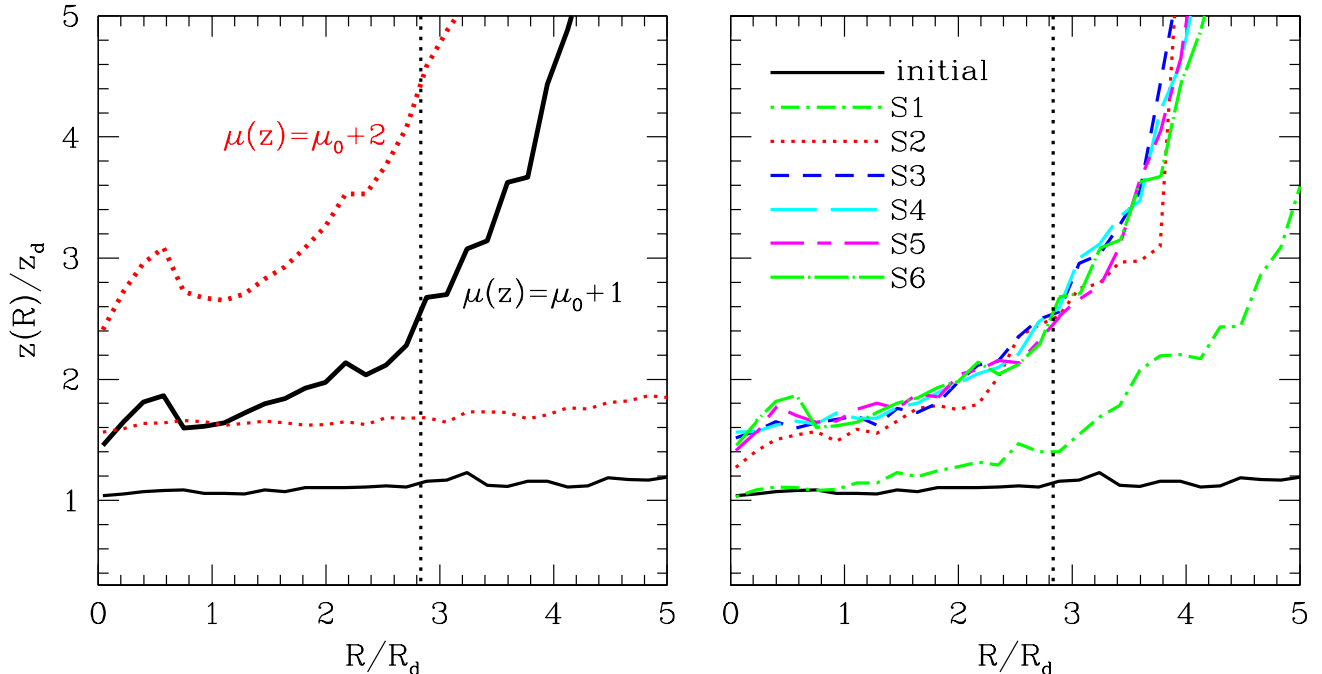


FIG. 6.— Disk flare. Scale height profiles, $z(R)$, of the disk viewed edge-on as a function of projected radius in units of the disk radial scale length, R_d . The scale height is defined to be the vertical distance from the disk plane where the surface brightness drops by 1 mag arcsec $^{-2}$ from its maximum along the $z = 0$ disk plane, $\mu(z) = \mu_0 + 1$ where $\mu_0 \equiv \mu(z = 0)$. Surface brightnesses are averaged about the $z = 0$ and $R = 0$ planes and all profiles are normalized to the initial disk scale height, z_d . *Left:* Scale height profiles for the initial (*thin lines*) and final disk (*thick lines*). *Solid lines* show results obtained using the above definition of scale height, while *dotted lines* correspond to scale heights defined to be the vertical position above $z = 0$ where the edge-on surface brightness falls off from the central value by 2 mag arcsec $^{-2}$. The initial disk is constructed with a constant scale height explaining why the corresponding curves are flat. The vertical dotted line indicates the location of the solar radius, R_\odot . A conspicuous flare is evident in the final disk beyond $\sim 2 - 3R_d$ as a result of the gravitational interaction with CDM substructure. *Right:* Evolution of the scale height profile of the disk. Various lines correspond to different satellite passages from S1 to S6 and scale heights are measured using the standard definition, $\mu(z) = \mu_0 + 1$. The encounters with the first two satellites give rise to a distinct flare in the outskirts of the disk. The combined effect of the remaining satellite passages (S3-S6) is much less dramatic indicating that the second, most massive encounter is responsible for setting the global disk structure. The inner disk appears much less susceptible to damage by the infalling subhalos owing to its large binding energy and presence of sinks of the orbital energy of satellites, such as the bulge component.

Now consider the impact of a dark subhalo with the disk. Some fraction of the orbital energy of the satellite ($\sim M_{\text{sat}} V_{\text{sat}}^2$, where V_{sat} is the orbital velocity), will be delivered as vertical kinetic energy to the disk. The disk will virialize on a dynamical timescale such that $t_z \simeq 0.5w_{dd} + w_{ds}$ (Toth & Ostriker 1992). When a subhalo passes through the disk, it frequently triggers global modes (e.g., spiral arms, warps, bars) which can be very efficient in redistributing its orbital energy throughout the disk (Sellwood et al. 1998). Moreover, if the infalling satellites are extended, like in the case of our simulations, most disk stars will also directly receive kinetic energy during the interaction. Both facts suggest that the orbital energy of an accreting subhalo will not be deposited locally at the point of impact as it was assumed by Toth & Ostriker (1992), but rather globally across the entire disk.

The simplest assumption for energy deposition is that it is roughly constant in radius such that $e_z(R) \rightarrow e_z(R) + \Delta e_z$, with Δe_z nearly independent of R . Moreover, due to the fact that rotational energy dominates over random motions in the plane of the disk, the predominant heating will be in the vertical direction. In this limit we can assume that the *projected* radial profiles of the disk and spheroid remain unchanged. The global change in vertical energy will demand that the scale height changes as:

$$\Delta z(R) \propto \frac{\Delta e_z}{\Sigma_d(R)[\alpha \Sigma_d(R) + 2z(R)\beta \bar{\rho}_s(R)]}. \quad (6)$$

In the limit where the disk surface density dominates the restoring force, the disk scale height will increase as $\Delta z(R) \propto \Sigma_d^{-2}(R)$. The presence of additional sinks of the orbital energy of satellites such as a massive, central bulge or a concentrated dark matter halo will further act to suppress the increase of scale height at small R . Indeed, as demonstrated in Paper II, a dense bulge is efficient in reducing the damaging effects of infalling subhalos on stellar disks.

Note also that once the disk is thickened to drive $z(R)$ to be quite large, we expect the second term in the denominator of eq. [6] to prevent any further vertical puffing of the disk. Generally speaking, this suggests that the most massive of the past encounters will set the scale height of the old thick disk, which is directly confirmed by the findings presented in the right panel of Figure 6.

It is particularly interesting to investigate how the pronounced flare we predict in our simulations would manifest in the surface brightness distribution of an edge-on disk. The relevant analysis is presented in Figure 7. This figure shows an edge-on “in-plane” ($z = 0$) surface brightness profile for both initial and final disk as a function of projected radius, R . The calculation assumes again a stellar mass-to-light ratio of $M_*/L = 3$. A steepening of the exponential slope can be seen in the profile of the final disk beyond a projected radius of $R \sim 10$ kpc. The entire surface brightness distribution of the final disk also decreases as a result of the encounters with the accreting satellites. Specifically, the surface brightness in

the outskirts ($R \sim 6R_d$) drops from $\mu \approx 27$ to $\mu \approx 29$ mag arcsec $^{-2}$.

Furthermore, the central surface brightness decreases from the initial value of $\mu \sim 21.2$ mag arcsec $^{-2}$ by $\Delta\mu \approx 0.6$ mag arcsec $^{-2}$. This is consistent with the decrease in the peak of the surface brightness profiles at $R = 0$ between initial and final disk seen in Figure 4. As we discussed earlier, this drop as well as the overall decrease of the brightness distribution can be explained by the fact that infalling satellites heat stars efficiently above the disk plane.

A low-surface brightness phenomenon seen in many disk galaxies is the tendency for exponential disks to be truncated at faint magnitudes (van der Kruit 1979; van der Kruit & Searle 1981; de Jong et al. 2007b). Such breaks were originally discovered in edge-on systems and appear to be less readily observed in face-on galaxies because of the line-of-sight projection and the associated lower surface brightness. It is important to emphasize that even though the behavior of the final edge-on disk depicted in Figure 7 resembles observed disk truncations, the steepening of the exponential slope disappears when the disk is viewed face-on. This suggests that the 3D stellar distribution does not actually truncate. Thus, the steepening of the surface brightness profile $\mu(z=0, R)$ reported here does not constitute a separate physical effect. On the contrary, it is a consequence of the flare.

In the outskirts, the binding energy of the disk is low and stars are efficiently heated above the disk plane by the infalling satellites. As a result, at large distances from the center, very little material remains in the disk plane which gives rise to a distinct drop-off in the surface brightness beyond $R \sim 3.5R_d$. On the other hand, the larger self-gravity of the inner, exponential disk and the presence of a massive bulge that acts as a sink of the satellites' orbital energy increase the robustness of the inner disk to accretion events and prohibit the development of such a break in the exponential slope at smaller radii.

4. DISCUSSION

4.1. Implications

We have demonstrated that encounters with CDM substructure can generate a wealth of morphological signatures in disk galaxies. These include conspicuous flares, central bars, low-surface brightness ring-like features in the outskirts of the disk, faint filamentary structures above the disk plane, and a complex vertical morphology that resembles the commonly adopted thin-thick disk profiles used in the analysis of disk galaxies. Font et al. (2001) and Gauthier et al. (2006) performed similar numerical investigations of the gravitational interaction between multi-component disk galaxies and infalling subhalos. Both of these investigations considered the population of surviving substructures at $z = 0$ and both studies found negligible effect on the global structure of the disk.

In particular, the aforementioned studies showed only mild evolution of the disk scale height as a function of radius due to the satellite population. In contrast, the present study reports substantial disk flaring stemming from the gravitational interaction with infalling CDM subhalos. As Figure 6 indicates, the flaring we find is associated with an increase of the disk scale height by more than a factor of 2 near the solar radius. The primary reason for this discrepancy is that we have followed the formation *history* of the host halo since $z \sim 1$, and consequently we have considered impacts of satellites onto the disk that are significantly more massive than those

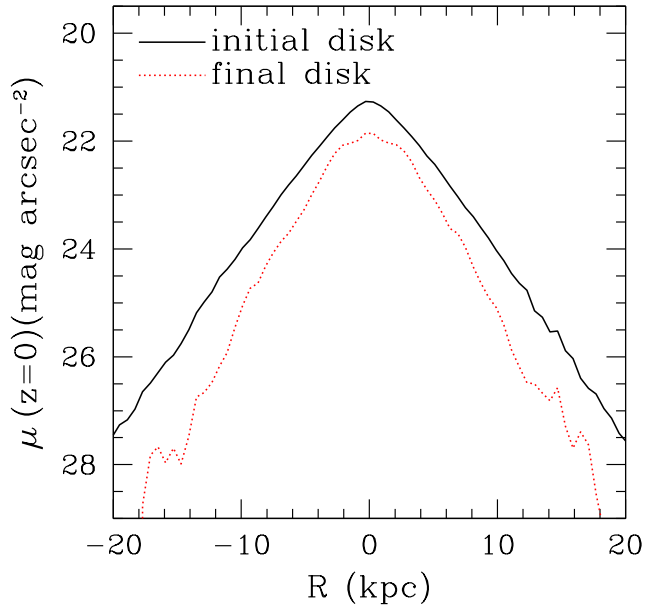


FIG. 7.— Edge-on surface brightness profiles of the stellar disk as a function of projected radius, R . The final disk (*dotted line*) exhibits a steepening in surface brightness distribution beyond $R \sim 3.5R_d$ compared to the initial disk (*solid line*). The peak of the surface brightness profile of the final disk decreases by $\Delta\mu \approx 0.6$ mag arcsec $^{-2}$ from the initial value. At large distances from the disk center a differential decrease in the surface brightness of $\Delta\mu \approx 2$ mag arcsec $^{-2}$ is established. Disk flaring due to infalling CDM substructures is responsible for generating breaks in the edge-on surface brightness profiles of galactic disks.

included in the numerical experiments of Font et al. (2001) and Gauthier et al. (2006).

This difference is critical because massive subhalos on highly eccentric orbits at early epochs become preferentially disrupted or suffer substantial mass loss during their orbital evolution, and so they are more likely to be absent from the $z = 0$ population (e.g., Zentner & Bullock 2003; Kravtsov et al. 2004; Gao et al. 2004). To capture these relatively short-lived objects, it is necessary to trace the interaction history of the central halo with nearby, massive systems as we have done here. Interestingly, orbital evolution models of the LMC and SMC using 3D velocities constrained by recent proper motion measurements suggest that these massive Galactic companions may currently be on their first passage about the MW (Besla et al. 2007). If confirmed, this is in line with the idea that massive objects would be present today only if they were recently-accreted.

As discussed in the introduction, it is tempting to associate the faint structures resulting from the satellite-disk interactions (Figures 3 and 5) with the recently-discovered complex disk phenomena seen in and around the MW and M31, and in other nearby and distant disk galaxies. Stellar counts in the MW from 2MASS and SDSS (Momany et al. 2006; Bell et al. 2007) identify stellar streams, many of which may be associated with recent merger or fly-by activity from Local Group galaxies, or other perturbations in the galactic disk. These studies also find a great deal more structure at radii beyond $R_{GC} \sim 10$ kpc (Bell et al. 2007), as well as a many-fold increase in the scale height of the disk, compared to that at the solar circle (Momany et al. 2006).

Figure 5 also illustrates that encounters with infalling

subhalos can generate warps in the outer disk. Warp excitation by tidal interactions with small companion galaxies constitutes an attractive mechanism. Indeed, it has recently been argued that the origin of the Galactic warp can be attributed to the interaction of the MW disk with the LMC (Weinberg & Blitz 2006). In more distant galaxies, extremely deep imaging has long revealed that multiple-component, thick-disk, and more extended diffuse structures are not limited to MW and M31 extending the applicability of our results beyond the Local Group (e.g., Sackett et al. 1994; Lequeux et al. 1998; Abe et al. 1999; Dalcanton & Bernstein 2002; Zibetti & Ferguson 2004; Dalcanton et al. 2005; Yoachim & Dalcanton 2006; de Jong et al. 2007a).

The ring-like feature shown in Figure 3 is particularly intriguing in light of the Monoceros structure in the MW. The present study suggests that rings of this kind are generated naturally as a result of satellite impacts, which can excite perturbations in *disk stars*. This phenomenon is different from the well-known “shell” structures that arise in stars that are *accreted* from dynamically cold systems that interact with larger galaxies (e.g., Hernquist & Quinn 1988; Helmi et al. 2003). In our simulations, the ring is caused by a perturbation within an initially cold disk.

In comparison to models that attempt to explain the Monoceros Ring and extended M31 disk structure using minor merger events that directly deposit stars, our scenario requires no special orbital configuration for the infalling satellites. In order to explain the origin of the aforementioned features, accreted-star models seem to require fairly circular, prograde, or (at least) low-inclination orbits (e.g., Helmi et al. 2003; Peñarrubia et al. 2005). In studies of *dissipationless* simulations, orbits of this type are quite rare for subhalos that penetrate deep into the host halo and interact with central disks (e.g., Ghigna et al. 1998; Knebe et al. 2004; Zentner et al. 2005a,b; Benson 2005). The subhalo orbital eccentricity distribution presented in the right panel of Figure 1 confirm this conclusion.

More circular orbits may be motivated by numerical experiments of satellite decay in disk-dominated or flattened systems that have reported rapid circularization of the orbit (e.g., Quinn & Goodman 1986; Peñarrubia et al. 2002; Meza et al. 2005). However, in the very least subhalo orbits will not be driven to nearly circular *prior* to an encounter with the central disk. The extended disk components and morphological features we report in the present study arise naturally in the context of a typical Λ CDM accretion history. Of course, a detailed kinematic analysis of the theoretical predictions will be important for testing whether rings of the type generated in our simulations can explain the observed MW Monoceros structure and M31 outer disk. We defer a detailed investigation of these considerations to future work.

In the context of distinctive observational signatures produced in stellar disks by accreting subhalos, an intriguing result is reported in Figure 6. This plot demonstrates that the scale height of the simulated disk increases with radius as a result of the gravitational interactions with infalling satellites. Indeed, disk flaring appears to be a natural result of encounters with CDM substructure and one of the most important observational consequences of the present study. Many late-type galaxies (including the MW and M31) exhibit a great deal of non-smooth “structure” in their stellar distributions, often with clear flaring at large galacto-centric radii.

Actual disk-flaring, such as that described in this paper, is seen in the MW in both the stellar disk

(López-Corredoira et al. 2002; Momany et al. 2006) and atomic hydrogen layer (e.g., Merrifield 1992; Nakanishi & Sofue 2003). Flaring is also observed in external galaxies seen edge-on, in their stellar light (e.g., de Grijs & Peletier 1997; Narayan & Jog 2002) (though more-rarely in lower-mass galaxies; de Grijs & Peletier 1997; Seth et al. 2005), as well as in H_I gas (e.g., Brinks & Burton 1984; Olling 1996; Matthews & Wood 2003). Extending the search for disk flaring in external systems would provide a new observational test for the Λ CDM paradigm and its competitors on non-linear, galactic scales, and thus offer unique opportunities to constrain cosmological models.

The structure and kinematics of galactic disks have long been recognized as a key constraint on structure formation models. Our results have intriguing implications for tests of the nature of dark matter through detailed observations of galactic structure. Alternatives to the standard CDM paradigm such as models with warm dark matter or decaying dark matter (e.g., Hogan & Dalcanton 2000; Avila-Reese et al. 2001; Cembranos et al. 2005; Kaplinghat 2005; Strigari et al. 2007b), or non-standard power spectra (e.g., Kamionkowski & Liddle 2000) predict substantially different accretion histories for MW-sized dark matter halos as well as different satellite abundances and structural properties (Zentner & Bullock 2003).

We have assessed the sensitivity of disk flaring to the density structure of the infalling systems by adopting satellite models with radically different density profiles, but requiring that the total bound mass of each object be exactly the same. Specifically, we repeated the first two satellite passages S1 and S2 modeling the infalling subhalos using a constant density core ($\rho(r) \propto r^{-\gamma}$, where $\gamma = 0$) and adopting the same outer, β , and intermediate, α , slopes of their CDM counterparts. The size of the density core was chosen to be approximately equal to 10% of the tidal radius of each subhalo ($\gtrsim 2$ kpc).

We find that cored satellites of equal bound mass produce much smaller amounts of disk flaring at the solar radius and at larger radii, and smaller overall disk morphological evolution compared to the standard CDM cosmological satellites whose density distribution is well described by a cusp slope of $\rho(r) \propto r^{-1}$. This is not unexpected since the former are more susceptible to mass loss and will, on average, approach and penetrate the disk with smaller amounts of orbital energy available to be converted into random motions of disk stars. These findings suggest that differences in the properties of the subhalo populations should be imprinted on the fine structure of disk galaxies.

Such differences can be used to provide fundamental constraints on structure formation theories by distinguishing between competing cosmological models. Indeed, specifically-designed surveys such as SEGUE and RAVE and planned revolutionary instruments like SIM and GAIA will be able to quantify the structure and kinematic properties of the MW disk. Moreover, future surveys like SEGUE-2, PanSTARRS, and LSST will provide ever more precise star-by-star maps of the Galaxy and multi-object spectrographs on thirty-meter class telescopes will enable star count maps for many galaxies in the local volume, similar to the maps being made for M31 and M33. Confronting the resulting data sets with theoretical predictions such as those of the present study will allow to test whether the detailed structure of galactic disks is as perturbed as predicted by the CDM paradigm.

We expect disk morphological evolution in MW-sized dark

matter halos, $M_{\text{vir}} \sim 10^{12} M_{\odot}$, to be driven by the few most massive satellite accretion events $M_{\text{sub}} \sim 10^{10-11} M_{\odot} \sim M_{\text{disk}}$. Indeed, mergers of this size dominate the mass buildup in galaxy-sized CDM halos (e.g., Zentner & Bullock 2003; Purcell et al. 2007). In addition, massive accretion events of this kind should have been relatively common since $z \sim 1$. We have shown this directly using our four well-resolved cosmological N -body halos in § 2.2. This result is corroborated by Stewart et al. (2007, in preparation) who use thousands of halos extracted from a Λ CDM N -body simulation ($\sigma_8 = 0.9$) to show that $\sim 80\%$ ($\sim 70\%$) of MW-sized objects should have accreted at least one subhalo with mass comparable to that of the disk in our controlled simulations, $M_{\text{sub}} > 0.02 M_{\text{vir}}$ ($> 0.05 M_{\text{vir}}$) since $z \sim 1$. Moreover, $\sim 60\%$ should have accreted a system with more than twice that mass over the same period ($> 0.1 M_{\text{vir}}$). Of course, the importance of these accretion events for both driving and altering disk morphologies will depend on the orbital evolution of the satellites once accreted into the host halo virial radius. However, given that dynamical friction will drive massive subhalos towards the central regions of the host halo within a few Gyr, these results serve as general motivation that significant central encounters should be fairly commonplace in the history of galaxy-sized halos.

The above discussion is particularly relevant in the context of the survival of thin, stellar disks to hierarchical satellite accretion. Figures 3, 4 and 5 illustrate that while infalling satellites substantially perturb stellar disks affecting their overall morphology, a significant thin disk component can survive bombardment by CDM substructure that is an appreciable fraction of the disk mass. Though most MW-sized galaxies are expected to have accreted an object at least as large as the disk itself since $z \sim 1$ (Figure 1) we have explicitly ignored these violent interactions in the present study in an attempt to be conservative. This is because our main goal was to examine the formation of distinct morphological features about a well-preserved disk galaxy similar to the MW and M31. An important future study will be to model the impact of a satellite as large as (or larger than) the disk itself in order to test the robustness of disks in this general framework. We intend to examine this issue fully in a forthcoming work. The results presented here provide some encouragement that such an experiment may not prove ruinous to the survival of thin disks in a Λ CDM universe.

Of specific concern for hierarchical models of structure formation is the prevalence of *old* (~ 10 Gyr) stars in the thin disk (e.g., Wyse 2001). Quillen & Garnett (2000) showed that the age-velocity dispersion relation in the solar neighborhood for disk stars was relatively flat between ~ 2 and ~ 10 Gyr, with a distinct jump in the velocity dispersion for older stars, as perhaps would be expected if thick disk formation were driven by a single ancient event. However, utilizing a sample ~ 75 times as large, Nordström et al. (2004) found a continuous increase of stellar velocity dispersion with age, and argued that ongoing heating could provide an explanation. Seabroke & Gilmore (2007) used the same data set and similarly concluded that vertical disk heating does not saturate at early times. Regardless, the age distribution of stars in the MW suggests that a significant fraction of the thin disk ($\sigma_z \lesssim 20 \text{ km s}^{-1}$) was in place by $z \sim 1$.

It is tempting to argue that the existence of an old, thin stellar disk would imply an absence of satellite impacts over a period that corresponds to at least the age of the oldest stars in the thin disk. If an impact occurs and destroys the disk, then

a thin disk component must be generated later by secondary processes such as gas inflow. This would suggest that thick disks originating during damaging encounters with substructures must be invariably older than the oldest stars in the thin disk, making thin and thick disks distinct in age as well as scale height. While this is true for the MW and other external galaxies, our results are consistent with a picture in which a thick disk arises naturally in the context of a typical Λ CDM accretion history while at the same time a substantial thin disk component survives the violent gravitational encounters with CDM substructure. Our results thus indicate that the absence of thick disks in significant fraction of disk galaxies, rather than ubiquitous thick disks, would represent a challenge for the CDM model.

The findings of the present study are especially relevant to the formation of thick disks. Thick disks constitute a ubiquitous component of disk galaxies (e.g., Dalcanton & Bernstein 2002; Yoachim & Dalcanton 2006) and several formation mechanisms have been proposed to explain their origin and properties. A growing body of evidence favors scenarios in which thick disk stars form initially either in the thin disk and then are dynamically heated to large scale heights by encounters with orbiting satellites (e.g., Quinn et al. 1993; Walker et al. 1996; Velazquez & White 1999) or in external galaxies and subsequently are deposited by accretion events at large scale heights (e.g., Abadi et al. 2003). The results presented in this paper suggest that a thick disk component may arise naturally as a result of gravitational interactions between an existing thin disk and infalling satellites with mass functions, density structures, and orbital distributions of the kind expected in the Λ CDM paradigm of structure formation. CDM substructure can thicken stellar disks (Figures 4 and 6) and should be regarded as being, in the very least, partially responsible for the origin of thick disks. As we show in Paper II, the stellar disk is substantially heated in all three directions by the encounters with infalling satellites S1-S6. Interestingly, the disk velocity ellipsoid at the solar radius, $R_{\odot} = 8$ kpc, increases from $(\sigma_R, \sigma_{\phi}, \sigma_z) = (31, 24, 17) \text{ km s}^{-1}$ to $(\sigma_R, \sigma_{\phi}, \sigma_z) \simeq (61, 49, 31) \text{ km s}^{-1}$. For reference, the velocity ellipsoid of the thick disk of the MW is estimated to be $\sim (46, 50, 35) \text{ km s}^{-1}$ by Chiba & Beers (2000) and $\sim (63, 39, 39) \text{ km s}^{-1}$ by Soubiran et al. (2003). However, it is important not to over-interpret this comparison because the final dispersions are calculated considering all stars instead of using only those that belong to the thick disk component according to the decomposition analysis of § 3.1

4.2. Caveats

Certainly our approach is not without drawbacks. The most evident one is that the present study used only four *dissipationless* MW-sized dark matter halos in order to derive “typical” orbits and merger histories, and the controlled simulations of satellite-disk interactions were based on the accretion history of just one of these host halos. It will be important to explore a range of accretion histories and orbital distributions of infalling objects using a larger sample of halos from cosmological N -body simulations. Moreover, since the orbital evolution of substructure once accreted into host halos will be influenced by baryonic processes, a self-consistent, hydrodynamical simulation of disk galaxy formation would be required to fully refine the conclusions presented here. Unfortunately, hydrodynamical simulations that produce statistical samples of realistic disk galaxies at $z = 0$ do not yet exist.

Despite the obvious limitations, several facts suggest that

our study has captured to at least a certain extent the amount of global morphological transformation that CDM satellites can cause to stellar disks. First, all four of the host halos we explored showed similar numbers of substantial central mergers, and their accretion histories are typical of systems in this mass range (e.g., Wechsler et al. 2002). Second, we used a *conservative* subset of one of the merger histories to seed the controlled satellite-disk encounter simulations, and neglected interactions with extremely massive subhalos that could prove ruinous to disk survival. If anything, the morphological response of most disks should be more pronounced compared to that we find here. Third, our numerical experiments took into account the effects of a realistic baryonic component on the orbital evolution of the infalling satellites by including a live central galaxy. Finally, most of the observational signatures on stellar disks (Figures 3, 4, 5, 6, and 7) were generated by the single most massive encounter ($M_{\text{sat}} \sim 0.6M_{\text{disk}}$, $r_{\text{tid}} \sim 20$ kpc, and $r_{\text{peri}} \lesssim 10$ kpc). We identify accretion events of this kind in all four of the host halo histories studied and, as discussed above, it is reasonable to expect that most MW-sized halos should have accreted numerous such systems since $z \sim 1$.

A second caveat is that we have neglected stellar components in the infalling satellites modeling the latter as pure dark matter subhalos. Thus, the present study is inadequate to address the contribution of satellite stars to the formation of the thick disk and elucidate their ability in driving existing or creating their own morphological signatures. Notwithstanding this limitation, the present work does demonstrate that dark matter subhalos can be capable of generating a wealth of morphological features in the simulated disks that resemble those seen in real galaxies. A third drawback is related to the fact that our models track only stars that were in place in a disk at $z \sim 1$, and therefore apply most directly to *old* disk stars. We have also adopted a primary disk galaxy model motivated by the present-day structure of the MW. A more complete investigation would have to include the ongoing formation of the disk.

Furthermore, we have only addressed the gravitational interaction of disk galaxies and dark matter substructures in the collisionless regime, a choice with obvious limitations. Spiral galaxies contain atomic and molecular gas which can absorb and subsequently radiate away part of the orbital energy deposited by the sinking satellites. Owing to this property, the heated gas component will eventually resettle to form a new thin disk consisting of a younger stellar population compared to that of the thick disk. Modeling the evolution of a dissipative component in the primary galaxy would be required to determine the extent to which the presence of gas can alter the dynamical effects of substructure on stellar disks. Given that the gas fraction in massive disk galaxies at $z \sim 0$ is typically low ($\sim 10\%$ of the stellar disk mass; Read & Trentham 2005), the role of a dissipative component in stabilizing the disks against the violent gravitational encounters with satellites may not be important, but this will depend sensitively on whether the gas content was higher in the past. Indeed, high gas-fractions at early times may be required to explain the formation of disk galaxies in a hierarchical universe (Robertson et al. 2006).

Finally, the present-day structure of galactic disks originates from a complex interplay of effects and a full explanation requires detailed knowledge of their star formation history and chemical evolution, amongst others. In fact, the thin and thick disk stars of the MW represent distinct

populations not only kinematically but also chemically (e.g., Wyse & Gilmore 1995; Bensby et al. 2005). Adding star formation as a further ingredient will provide the opportunity to track ongoing star formation in an ever re-forming thin disk and refine the conclusions presented here. All of these effects will be discussed in forthcoming works.

5. SUMMARY

Using high-resolution, fully self-consistent dissipationless N -body simulations we have examined the observational signatures of the accretion of substructures onto thin disk galaxies in the context of the Λ CDM paradigm of structure formation. Our simulation campaign utilizes cosmological simulations of the formation of MW-sized dark matter halos to derive the properties of subhalo populations and controlled numerical experiments of consecutive satellite encounters with an initially-thin MW-type disk galaxy. The present study extends and expands upon past numerical investigations into the interaction between disk galaxies and merging satellites in at least three major respects.

First, we incorporate a model in which the infalling satellite populations are truly representative of those accreted and possibly destroyed in the past, instead of the $z = 0$ surviving substructure present in a CDM halo. Second, the primary disk galaxy models are fully self-consistent and flexible enough to permit detailed modeling of actual galaxies. Third, individual satellites are initialized according to the internal structure of subhalos culled from high-resolution cosmological simulations. All of these elements inherent in the modeling ensure that the numerical experiments of satellite-disk encounters were performed with a high degree of realism.

In contrast to what can be inferred from statistics of the present-day substructure populations in galaxy-sized CDM halos, encounters between massive subhalos ($M_{\text{sat}} \gtrsim 0.2M_{\text{disk}}$) and central disks should be common occurrences in standard Λ CDM since $z \sim 1$. Most of the difference is caused by the fact that satellites that pass closest to the halo center at early times are precisely those that are most likely to suffer significant mass loss or become tidally disrupted. As subhalos on highly eccentric orbits lose mass, the fraction of massive satellites with small orbital pericenters declines with redshift so that few remain by $z = 0$. The specific merger history we studied involved 6 accretion events of satellites with masses, orbital pericenters, and tidal radii of $7.4 \times 10^9 \lesssim M_{\text{sat}}/M_{\odot} \lesssim 2 \times 10^{10}$, $r_{\text{peri}} \lesssim 20$ kpc, and $r_{\text{tid}} \gtrsim 20$ kpc, respectively, over a ~ 8 Gyr period. The morphological impact of these events on an initially-thin ($z_d = 0.4$ kpc) MW-type disk galaxy ($M_{\text{disk}} \approx 3.5 \times 10^{10}M_{\odot}$) included the following signatures, many of which resemble features seen in the MW and M31, and in other disk galaxies.

- The development of a “thick” disk component and the survival of a significant “thin” disk component, as characterized by standard “thin-thick” disk decomposition analysis.
- The growth of a strong central bar.
- The production of a pronounced flare at intermediate and large radii, particularly visible at low surface brightness levels.
- The formation of long-lived, low-surface brightness ring-like features in the outskirts of the disk and faint filamentary structures that develop above the disk plane.

We conclude that gravitational interactions between existing thin disks and CDM substructure should be at least partially responsible for the formation of thick disks, disk flares, central bars, low-surface brightness ring-like configurations and faint filamentary structures around disk galaxies. The fact that many of these features appear ubiquitous in real galaxies is encouraging for the Λ CDM paradigm of structure formation.

The authors are grateful to Andrew Benson, Annette Ferguson, Andreea Font, Kathryn Johnston, Lucio Mayer, Ben Moore, Jorge Peñarrubia, Tom Quinn, Steven Snell, Joachim Stadel, and Octavio Valenzuela for many stimulating discussions. SK would like to thank Frank van den Bosch for communicating unpublished results, and John Dubinski and Larry Widrow for kindly making available the software used to set up the primary galaxy model. SK, JSB, and AVK acknowledge the Aspen Center for Physics for hosting the summer workshop “Deconstructing the Local Group – Dissecting Galaxy Formation in our Own Background” where some

of this work was completed. SK is also grateful to the Research Center for Astronomy and Applied Mathematics at the Academy of Athens for their hospitality during a visit when the final stages of this work were completed. SK is supported by a Kavli Institute for Particle Astrophysics and Cosmology (KIPAC) Postdoctoral Fellowship at Stanford University. ARZ is funded by the Kavli Institute for Cosmological Physics (KICP) at The University of Chicago and The National Science Foundation under grant NSF PHY 0114422 and through the Astronomy and Astrophysics Postdoctoral Fellowship Program under grant AST 0602122. AVK is supported by the NSF grants AST-0239759 and AST-0507596, and by KICP. The work of LAM was carried out at the Jet Propulsion Laboratory, California Institute of Technology under a contract with NASA. The numerical simulations were performed on the zBox supercomputer at The University of Zürich and on the Cosmos cluster at the Jet Propulsion Laboratory. This research made use of the NASA Astrophysics Data System.

REFERENCES

- Abadi, M. G., Navarro, J. F., & Steinmetz, M. 2006, *MNRAS*, 365, 747
 Abadi, M. G., Navarro, J. F., Steinmetz, M., & Eke, V. R. 2003, *ApJ*, 591, 499
 Abe, F. et al. 1999, *AJ*, 118, 261
 Ardi, E., Tsuchiya, T., & Burkert, A. 2003, *ApJ*, 596, 204
 Avila-Reese, V., Colín, P., Valenzuela, O., D’Onghia, E., & Firmani, C. 2001, *ApJ*, 559, 516
 Barth, A. J. 2007, *AJ*, 133, 1085
 Bell, E. F. et al. 2007, *ApJ* submitted (astro-ph/0706.0004)
 Belokurov, V. et al. 2006, *ApJ*, 642, L137
 Bensby, T., Feltzing, S., Lundström, I., & Ilyin, I. 2005, *A&A*, 433, 185
 Benson, A. J. 2005, *MNRAS*, 358, 551
 Benson, A. J., Lacey, C. G., Frenk, C. S., Baugh, C. M., & Cole, S. 2004, *MNRAS*, 351, 1215
 Besla, G., Kallivayalil, N., Hernquist, L., Robertson, B., Cox, T. J., van der Marel, R. P., & Alcock, C. 2007, *ApJ* submitted (astro-ph/0703196)
 Binney, J. & Tremaine, S. 1987, *Galactic dynamics* (Princeton, NJ, Princeton University Press, 1987, 747 p.)
 Blumenthal, G. R., Faber, S. M., Primack, J. R., & Rees, M. J. 1984, *Nature*, 311, 517
 Brinks, E. & Burton, W. B. 1984, *A&A*, 141, 195
 Brook, C. B., Kawata, D., Gibson, B. K., & Flynn, C. 2004, *MNRAS*, 349, 52
 Brown, T. M., Smith, E., Ferguson, H. C., Rich, R. M., Guhathakurta, P., Renzini, A., Sweigart, A. V., & Kimble, R. A. 2006, *ApJ*, 652, 323
 Bullock, J. S. & Johnston, K. V. 2005, *ApJ*, 635, 931
 Bullock, J. S., Kravtsov, A. V., & Weinberg, D. H. 2001, *ApJ*, 548, 33
 Cembranos, J. A., Feng, J. L., Rajaraman, A., & Takayama, F. 2005, *Physical Review Letters*, 95, 181301
 Chiba, M. & Beers, T. C. 2000, *AJ*, 119, 2843
 Cole, S. & Lacey, C. 1996, *MNRAS*, 281, 716
 Combes, F. & Sanders, R. H. 1981, *A&A*, 96, 164
 Conn, B. C., Martin, N. F., Lewis, G. F., Ibata, R. A., Bellazzini, M., & Irwin, M. J. 2005, *MNRAS*, 364, L13
 Dalcanton, J. J. & Bernstein, R. A. 2002, *AJ*, 124, 1328
 Dalcanton, J. J., Seth, A., & Yoachim, P. 2005, in *Proceedings of "Island Universes: Structure and Evolution of Disk Galaxies"*, Terschelling, the Netherlands (astro-ph/0509700)
 de Grijs, R. & Peletier, R. F. 1997, *A&A*, 320, L21
 de Jong, R. S. et al. 2007a, in the proceedings of IAUS 241: "Stellar Populations as Building Blocks of Galaxies" (astro-ph/0702168)
 —. 2007b, *ApJL* accepted (astro-ph/0708.0826)
 Dehnen, W. & Binney, J. 1998, *MNRAS*, 294, 429
 Faria, D., Johnson, R. A., Ferguson, A. M. N., Irwin, M. J., Ibata, R. A., Johnston, K. V., Lewis, G. F., & Tanvir, N. R. 2007, *AJ*, 133, 1275
 Ferguson, A. 2007, in *Proceedings of "From Stars to Galaxies: Building the Pieces to Build up the Universe"*, eds. Vallenari et al, *ASP Conf Series* (astro-ph/0702224)
 Ferguson, A. M. N., Johnson, R. A., Faria, D. C., Irwin, M. J., Ibata, R. A., Johnston, K. V., Lewis, G. F., & Tanvir, N. R. 2005, *ApJ*, 622, L109
 Font, A. S., Navarro, J. F., Stadel, J., & Quinn, T. 2001, *ApJ*, 563, L1
 Gao, L., White, S. D. M., Jenkins, A., Stoehr, F., & Springel, V. 2004, *MNRAS*, 355, 819
 Gauthier, J.-R., Dubinski, J., & Widrow, L. M. 2006, *ApJ*, 653, 1180
 Ghigna, S., Moore, B., Governato, F., Lake, G., Quinn, T., & Stadel, J. 1998, *MNRAS*, 300, 146
 Gilmore, G., Wyse, R. F. G., & Norris, J. E. 2002, *ApJ*, 574, L39
 Gnedin, N. Y. & Kravtsov, A. V. 2006, *ApJ*, 645, 1054
 Gordon, K. D. et al. 2006, *ApJ*, 638, L87
 Governato, F., Mayer, L., Wadsley, J., Gardner, J. P., Willman, B., Hayashi, E., Quinn, T., Stadel, J., & Lake, G. 2004, *ApJ*, 607, 688
 Governato, F., Willman, B., Mayer, L., Brooks, A., Stinson, G., Valenzuela, O., Wadsley, J., & Quinn, T. 2007, *MNRAS*, 374, 1479
 Grillmair, C. J. 2006a, *ApJ*, 645, L37
 —. 2006b, *ApJ*, 651, L29
 Grillmair, C. J. & Dionatos, O. 2006, *ApJ*, 643, L17
 Hayashi, H. & Chiba, M. 2006, *PASJ*, 58, 835
 Helmi, A., Navarro, J. F., Meza, A., Steinmetz, M., & Eke, V. R. 2003, *ApJ*, 592, L25
 Hernquist, L. 1990, *ApJ*, 356, 359
 —. 1993, *ApJS*, 86, 389
 Hernquist, L. & Quinn, P. J. 1988, *ApJ*, 331, 682
 Hogan, C. J. & Dalcanton, J. J. 2000, *PRD*, 62, 063511
 Huang, S. & Carlberg, R. G. 1997, *ApJ*, 480, 503
 Ibata, R., Chapman, S., Ferguson, A. M. N., Lewis, G., Irwin, M., & Tanvir, N. 2005, *ApJ*, 634, 287
 Ibata, R., Irwin, M., Lewis, G., Ferguson, A. M. N., & Tanvir, N. 2001a, *Nature*, 412, 49
 Ibata, R., Irwin, M., Lewis, G. F., & Stolte, A. 2001b, *ApJ*, 547, L133
 Ibata, R., Lewis, G. F., Irwin, M., Totten, E., & Quinn, T. 2001c, *ApJ*, 551, 294
 Ibata, R., Martin, N. F., Irwin, M., Chapman, S., Ferguson, A. M. N., Lewis, G. F., & McConnachie, A. W. 2007, *ApJ* submitted (astro-ph/0704.1318), 704
 Ibata, R. A., Gilmore, G., & Irwin, M. J. 1994, *Nature*, 370, 194
 Ibata, R. A., Irwin, M. J., Lewis, G. F., Ferguson, A. M. N., & Tanvir, N. 2003, *MNRAS*, 340, L21
 Ivezić, Ž. et al. 2000, *AJ*, 120, 963
 Johnston, K. V., Spergel, D. N., & Hernquist, L. 1995, *ApJ*, 451, 598
 Juric, M. et al. 2005, *ArXiv Astrophysics e-prints* (astro-ph/0510520)
 Kalirai, J. S., Guhathakurta, P., Gilbert, K. M., Reitzel, D. B., Majewski, S. R., Rich, R. M., & Cooper, M. C. 2006, *ApJ*, 641, 268
 Kamionkowski, M. & Liddle, A. R. 2000, *Physical Review Letters*, 84, 4525
 Kaplinghat, M. 2005, *Phys. Rev. D*, 72, 063510
 Kazantzidis, S., Magorrian, J., & Moore, B. 2004a, *ApJ*, 601, 37
 Kazantzidis, S., Mayer, L., Mastropietro, C., Diemand, J., Stadel, J., & Moore, B. 2004b, *ApJ*, 608, 663
 Kazantzidis, S., Zentner, A. R., & Nagai, D. 2006, in *EAS Publications Series*, ed. G. A. Mamon, F. Combes, C. Deffayet, & B. Fort, 65–68
 Kent, S. M., Dame, T. M., & Fazio, G. 1991, *ApJ*, 378, 131

- Klypin, A., Kravtsov, A. V., Valenzuela, O., & Prada, F. 1999, *ApJ*, 522, 82
- Klypin, A., Zhao, H., & Somerville, R. S. 2002, *ApJ*, 573, 597
- Klypin, A. A., Kravtsov, A. V., Bullock, J. S., & Primack, J. R. 2001, *ApJ*, 554, 903
- Knebe, A., Gill, S. P. D., Gibson, B. K., Lewis, G. F., Ibata, R. A., & Dopita, M. A. 2004, *ApJ*, 603, 7
- Kravtsov, A. V. 1999, PhD thesis, New Mexico State University
- Kravtsov, A. V., Gnedin, O. Y., & Klypin, A. A. 2004, *ApJ*, 609, 482
- Kravtsov, A. V., Klypin, A. A., Bullock, J. S., & Primack, J. R. 1998, *ApJ*, 502, 48
- Kravtsov, A. V., Klypin, A. A., & Khokhlov, A. M. 1997, *ApJS*, 111, 73
- Kuijken, K. & Dubinski, J. 1995, *MNRAS*, 277, 1341
- Larsen, J. A. & Humphreys, R. M. 2003, *AJ*, 125, 1958
- Lequeux, J., Combes, F., Dantel-Fort, M., Cuillandre, J.-C., Fort, B., & Mellier, Y. 1998, *A&A*, 334, L9
- Libeskind, N. I., Cole, S., Frenk, C. S., Okamoto, T., & Jenkins, A. 2007, *MNRAS*, 374, 16
- López-Corredoira, M., Cabrera-Lavers, A., Garzón, F., & Hammersley, P. L. 2002, *A&A*, 394, 883
- Lütticke, R., Dettmar, R.-J., & Pohlen, M. 2000, *A&AS*, 145, 405
- Majewski, S. R., Skrutskie, M. F., Weinberg, M. D., & Ostheimer, J. C. 2003, *ApJ*, 599, 1082
- Martin, N. F., Ibata, R. A., Bellazzini, M., Irwin, M. J., Lewis, G. F., & Dehnen, W. 2004, *MNRAS*, 348, 12
- Martínez-Delgado, D., Butler, D. J., Rix, H.-W., Franco, V. I., Peñarrubia, J., Alfaro, E. J., & Dinescu, D. I. 2005, *ApJ*, 633, 205
- Mastropietro, C., Moore, B., Mayer, L., Wadsley, J., & Stadel, J. 2005, *MNRAS*, 363, 509
- Mateo, M. L. 1998, *ARA&A*, 36, 435
- Matthews, L. D. & Wood, K. 2003, *ApJ*, 593, 721
- Mayer, L., Kazantzidis, S., Mastropietro, C., & Wadsley, J. 2007, *Nature*, 445, 738
- Mendez, R. A. & Guzman, R. 1998, *A&A*, 333, 106
- Merrifield, M. R. 1992, *AJ*, 103, 1552
- Meza, A., Navarro, J. F., Abadi, M. G., & Steinmetz, M. 2005, *MNRAS*, 359, 93
- Moitinho, A., Vázquez, R. A., Carraro, G., Baume, G., Giorgi, E. E., & Lyra, W. 2006, *MNRAS*, 368, L77
- Momany, Y., Zaggia, S., Gilmore, G., Piotto, G., Carraro, G., Bedin, L. R., & de Angeli, F. 2006, *A&A*, 451, 515
- Momany, Y., Zaggia, S. R., Bonifacio, P., Piotto, G., De Angeli, F., Bedin, L. R., & Carraro, G. 2004, *A&A*, 421, L29
- Moore, B., Ghigna, S., Governato, F., Lake, G., Quinn, T., Stadel, J., & Tozzi, P. 1999, *ApJ*, 524, L19
- Moore, B., Kazantzidis, S., Diemand, J., & Stadel, J. 2004, *MNRAS*, 354, 522
- Nakanishi, H. & Sofue, Y. 2003, *PASJ*, 55, 191
- Narayan, C. A. & Jog, C. J. 2002, *A&A*, 390, L35
- Navarro, J. F., Frenk, C. S., & White, S. D. M. 1995, *MNRAS*, 275, 56
- . 1996, *ApJ*, 462, 563
- Newberg, H. J., Mayeur, P. A., Yanny, B., & the SEGUE collaboration. 2006, *Memorie della Societa Astronomica Italiana*, 77, 1049
- Newberg, H. J. et al. 2002, *ApJ*, 569, 245
- Nordström, B. et al. 2004, *A&A*, 418, 989
- Olling, R. P. 1996, *AJ*, 112, 457
- Peñarrubia, J., Kroupa, P., & Boily, C. M. 2002, *MNRAS*, 333, 779
- Peñarrubia, J., McConnachie, A., & Babul, A. 2006, *ApJ*, 650, L33
- Peñarrubia, J. et al. 2005, *ApJ*, 626, 128
- Prada, F., Klypin, A. A., Simonneau, E., Betancort-Rijo, J., Patiri, S., Gottlöber, S., & Sanchez-Conde, M. A. 2006, *ApJ*, 645, 1001
- Purcell, C. W., Bullock, J. S., & Zentner, A. R. 2007, *ApJ* accepted (astro-ph/0703004)
- Quillen, A. C. & Garnett, D. R. 2000, *ApJ* submitted (astro-ph/0004210)
- Quinn, P. J. & Goodman, J. 1986, *ApJ*, 309, 472
- Quinn, P. J., Hernquist, L., & Fullagar, D. P. 1993, *ApJ*, 403, 74
- Read, J. I. & Trentham, N. 2005, *Royal Society of London Philosophical Transactions Series A*, 363, 2693
- Robertson, B., Bullock, J. S., Cox, T. J., Di Matteo, T., Hernquist, L., Springel, V., & Yoshida, N. 2006, *ApJ*, 645, 986
- Robertson, B., Yoshida, N., Springel, V., & Hernquist, L. 2004, *ApJ*, 606, 32
- Rocha-Pinto, H. J., Majewski, S. R., Skrutskie, M. F., & Crane, J. D. 2003, *ApJ*, 594, L115
- Rocha-Pinto, H. J., Majewski, S. R., Skrutskie, M. F., Patterson, R. J., Nakanishi, H., Muñoz, R. R., & Sofue, Y. 2006, *ApJ*, 640, L147
- Sackett, P. D., Morrison, H. L., Harding, P., & Boroson, T. A. 1994, *Nature*, 370, 441
- Schommer, R. A., Suntzeff, N. B., Olszewski, E. W., & Harris, H. C. 1992, *AJ*, 103, 447
- Seabroke, G. M. & Gilmore, G. 2007, *MNRAS* accepted (astro-ph/0707.1027)
- Sellwood, J. A., Nelson, R. W., & Tremaine, S. 1998, *ApJ*, 506, 590
- Seth, A. C., Dalcanton, J. J., & de Jong, R. S. 2005, *AJ*, 130, 1574
- Siegel, M. H., Majewski, S. R., Reid, I. N., & Thompson, I. B. 2002, *ApJ*, 578, 151
- Sommer-Larsen, J. & Dolgov, A. 2001, *ApJ*, 551, 608
- Sommer-Larsen, J., Götz, M., & Portinari, L. 2003, *ApJ*, 596, 47
- Soubiran, C., Bienaymé, O., & Siebert, A. 2003, *A&A*, 398, 141
- Spitzer, L. J. 1942, *ApJ*, 95, 329
- Stadel, J. G. 2001, Ph.D. Thesis, Univ. of Washington
- Stoehr, F., White, S. D. M., Tormen, G., & Springel, V. 2002, *MNRAS*, 335, L84
- Strigari, L. E., Bullock, J. S., Kaplinghat, M., Diemand, J., Kuhlen, M., & Madau, P. 2007a, *ApJ* accepted (astro-ph/0704.1817)
- Strigari, L. E., Kaplinghat, M., & Bullock, J. S. 2007b, *Phys. Rev. D*, 75, 061303
- Thacker, R. J. & Couchman, H. M. P. 2001, *ApJ*, 555, L17
- Toth, G. & Ostriker, J. P. 1992, *ApJ*, 389, 5
- van der Kruit, P. C. 1979, *A&AS*, 38, 15
- van der Kruit, P. C. & Searle, L. 1981, *A&A*, 95, 105
- Velazquez, H. & White, S. D. M. 1999, *MNRAS*, 304, 254
- Walker, I. R., Mihos, J. C., & Hernquist, L. 1996, *ApJ*, 460, 121
- Wechsler, R. H., Bullock, J. S., Primack, J. R., Kravtsov, A. V., & Dekel, A. 2002, *ApJ*, 568, 52
- Weil, M. L., Eke, V. R., & Efstathiou, G. 1998, *MNRAS*, 300, 773
- Weinberg, M. D. & Blitz, L. 2006, *ApJ*, 641, L33
- White, S. 2000, in *KITP: Blackboard Lunch Series*
- Widrow, L. M. & Dubinski, J. 2005, *ApJ*, 631, 838
- Wyse, R. F. G. 2001, in *ASP Conf. Ser. 230: Galaxy Disks and Disk Galaxies*, ed. J. G. Funes & E. M. Corsini, 71–80
- Wyse, R. F. G. & Gilmore, G. 1995, *AJ*, 110, 2771
- Yanny, B. et al. 2000, *ApJ*, 540, 825
- . 2003, *ApJ*, 588, 824
- Yoachim, P. & Dalcanton, J. J. 2006, *AJ*, 131, 226
- Zentner, A. R., Berlind, A. A., Bullock, J. S., Kravtsov, A. V., & Wechsler, R. H. 2005a, *ApJ*, 624, 505
- Zentner, A. R. & Bullock, J. S. 2003, *ApJ*, 598, 49
- Zentner, A. R., Kravtsov, A. V., Gnedin, O. Y., & Klypin, A. A. 2005b, *ApJ*, 629, 219
- Zhao, H. 1996, *MNRAS*, 278, 488
- Zibetti, S. & Ferguson, A. M. N. 2004, *MNRAS*, 352, L6